Supplementary Information

Vitrification of non-meltable zeolitic-imidazolate frameworks

Mohamed. A. Ali[a]*, Zhihua Qiao[b], Wessel. M. W. Winters[c], Biao Cai[d], Moushira. A. Mohamed[a], Yanfei Zhang[e], Xiaofeng Liu[f]*, Yuanzheng Yue[c]*, Jianrong Qiu[a]*

[a]State Key Laboratory of Modern Optical Instrumentation, College of Optical Science and Engineering, Zhejiang University, Hangzhou 310027, China.

[b]State Key Laboratory of Separation Membranes and Membrane Processes, Tiangong University, Tianjin, 300387, China.

[c]Department of Chemistry and Bioscience, Aalborg University, DK-9220 Aalborg, Denmark.

[d]School of Metallurgy and Materials, University of Birmingham, B15 2TT, UK.

[e]School of Materials Science and Engineering, Qilu University of Technology (Shandong Academy of Sciences), Jinan 250353, China.

[f]School of Materials Science and Engineering, Zhejiang University, Hangzhou 310027, China.

*Corresponding author. E-mail: qjr@zju.edu.cn (J.Q.); yy@bio.aau.dk (Y.Y.); xfliu@zju.edu.cn (X.L.) mohamedali@zju.edu.cn (M.A.A).

Contents

Supplementary Figures

Supplementary Tables

Table S4. Summary of the porosity characteristics of ZIF-7 and ZIF-8 foams derived from ZIF-7 and ZIF-8 crystals.

Supplementary Texts

I. Structral differences between ZIF crystals, ZNIC liquids, and ZIF foams.

II. Gas adsorption of ZIF crystals and ZIF foams.

Supplementary References

Abbreviations

PXRD	Powder X-ray diffraction
ZIF	Zeolitic imidazolate framework
ZNIC	Zinc nitrate imidazole complex
TGA	Thermogravimetric analysis
DSC	Differential scanning calorimetry
T_d	Decomposition temperature
MAS	Magic-angle-spinning
FTIR	Fourier transform infrared spectroscopy
MS	Mass spectroscopy
NMR	Nuclear magnetic resonance
HR-TEM	High resolution transmission electron microscope
SAED	Selected-area electron diffraction
PDF	Pair distribution function
ICP-MS	Inductively coupled plasma mass spectrometry
SEM	Scanning electron microscope
EDS	Energy dispersive spectroscopy
DFT	Density functional theory
BET	Brunauer–Emmett–Teller
PALS	Positron annihilation lifetime spectroscopy
τ_3	Lifetime
I_3	Intensity

D_3 Pore diameter

V_f Pore volume

FFV Fractional free volume

bIm Benzimidazole

mIm 2-methylimidazole

MUV-24 Fe-based ZIF ($Fe(Im)_2$)

ZIF-62 $Zn(Im)_{1.75}(bIm)_{0.25}$, Im = imidazolate

ZIF-76 $Zn(Im)_{1.62}(CbIm)_{0.8}$, CbIm = 6-chlorobenzimidazolate

ZIF-4 $Zn(Im)_2$

ZIF-UC-2 $Zn(Im)_{1.87}(6\text{-Cl-5-FbIm})_{0.13}$, 6-Cl-5-FbIm = 6-chloro-5-fluoro-benzimidazolate

ZIF-7 $Zn(bIm)_2$

ZIF-8 $Zn(mIm)_2$

ZIF-95 $Zn(CbIm)_2$

IL Ionic liquid

RT Room temperature

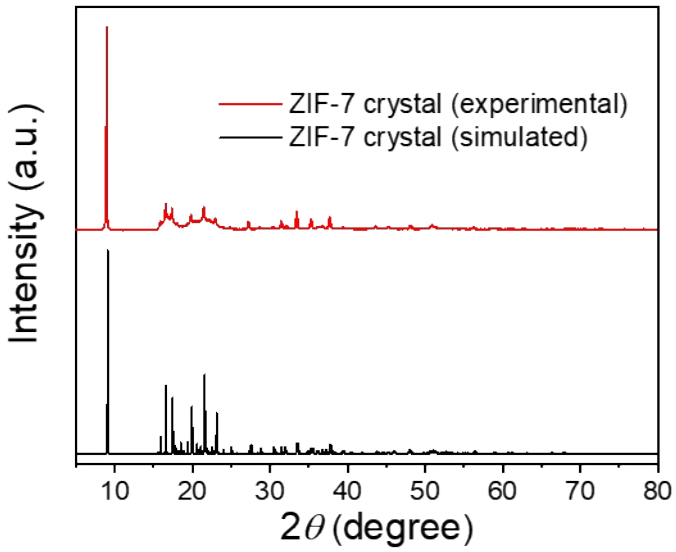

Fig. S1. PXRD patterns of the as-synthesized and simulated ZIF-7 crystal by the solvothermal method.

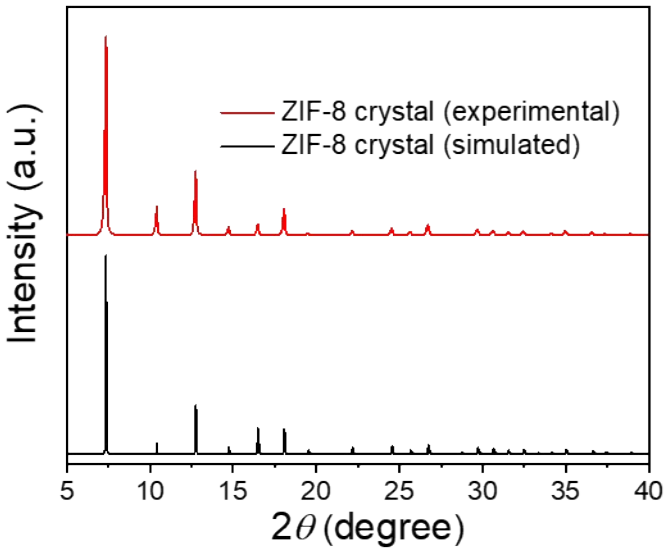

Fig. S2. PXRD patterns of the as-synthesized and simulated ZIF-8 crystal by the solvothermal method.

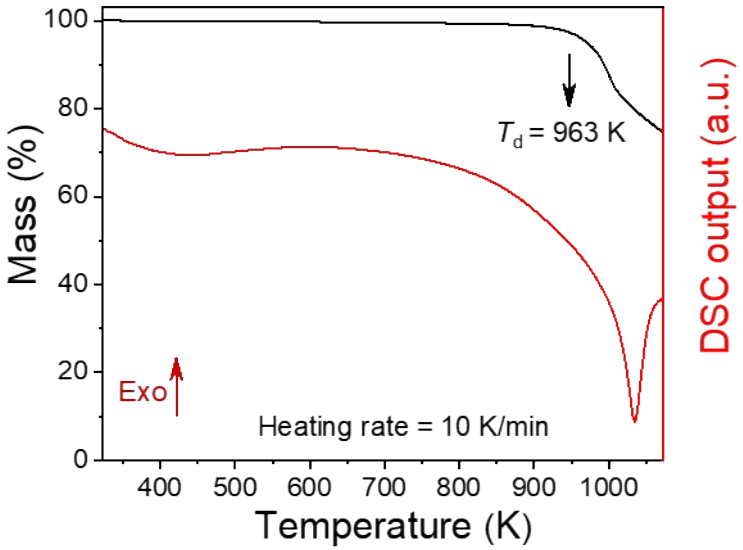

Fig. S3. DSC-TGA traces of the as-synthesized ZIF-7 crystal.

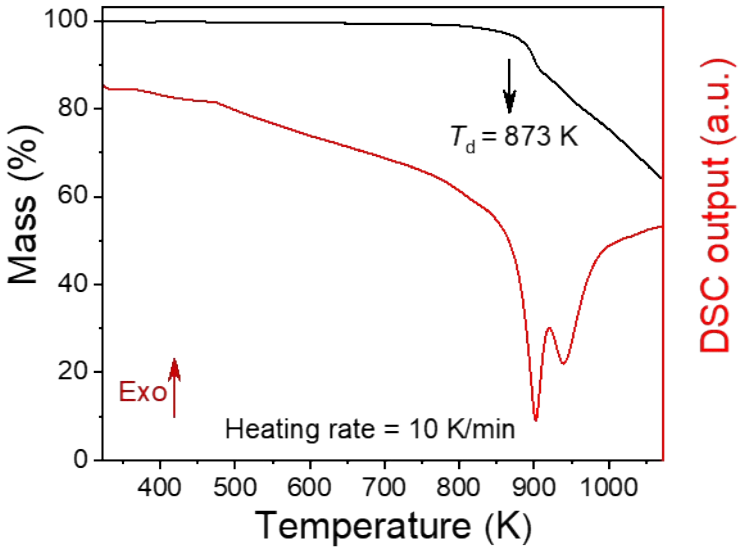

Fig. S4. DSC-TGA traces of the as-synthesized ZIF-8 crystal.

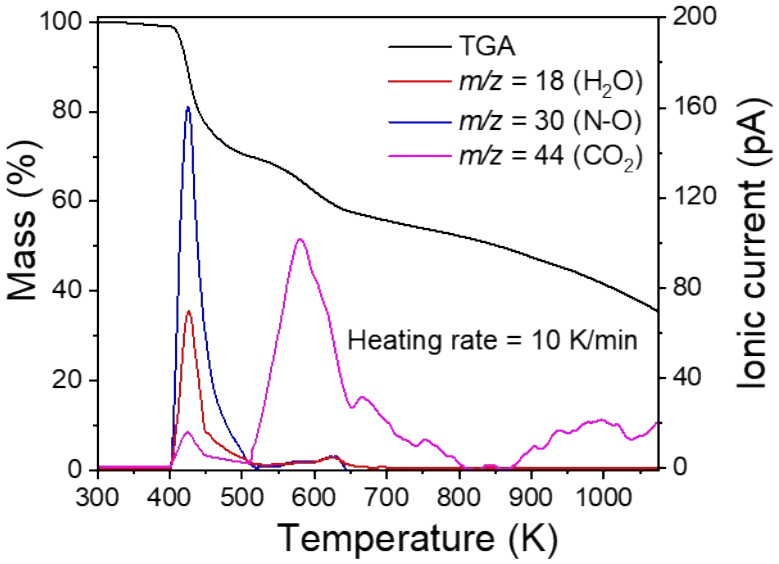

Fig. S5. TGA-MS trace of the as-synthesized ZNIC-8 liquid, demonstrating the H_2O, NO, and CO_2 molecules are released at temperatures above 400 K.

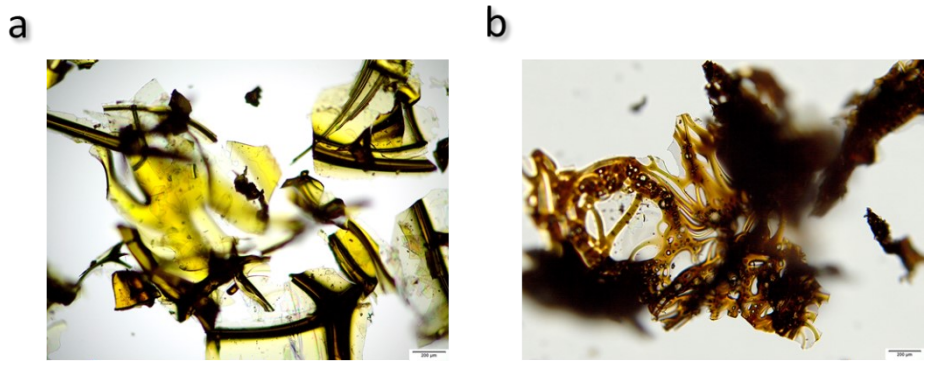

Fig. S6. Optical image of the as-synthesized (a) ZIF-7 foam and (b) ZIF-8 foam at RT.

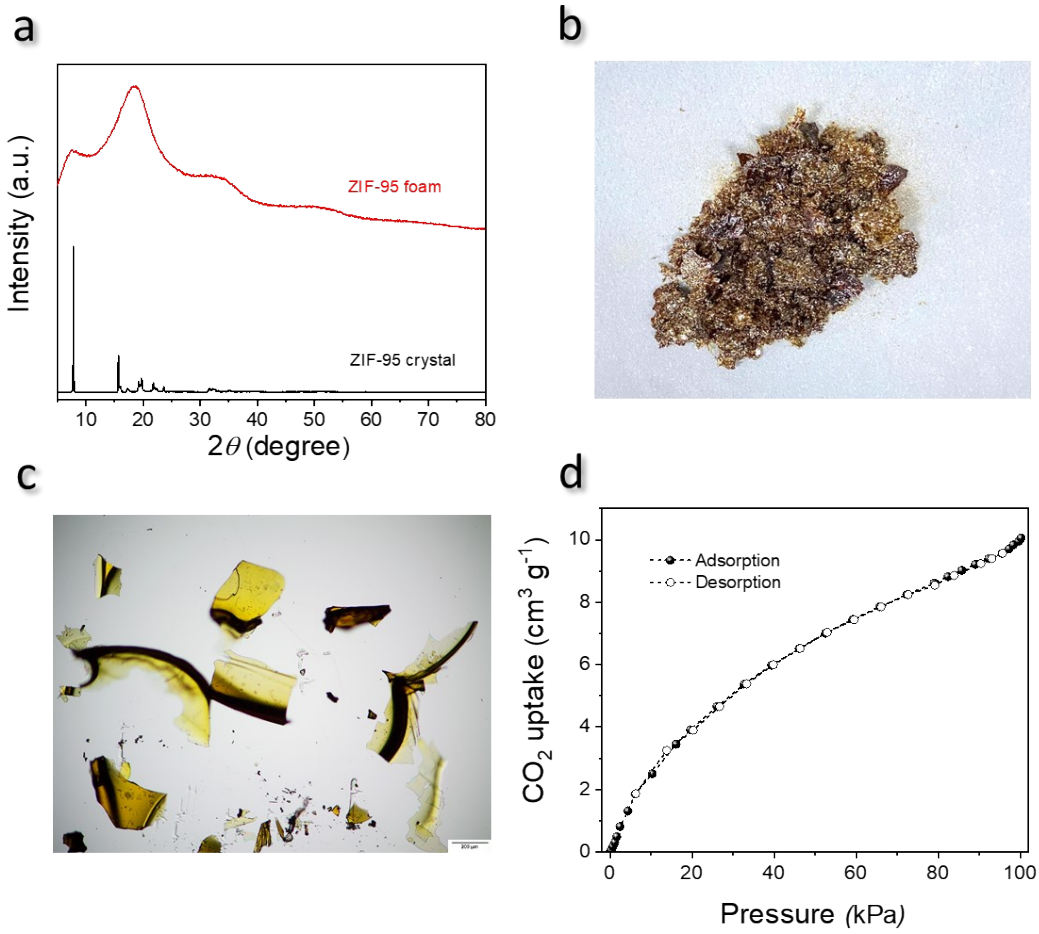

Fig. S7. (a) PXRD patterns of the as-synthesized ZIF-95 crystal and ZIF-95 foam at RT. (b) Photograph and (c) optical image of the as-synthesized ZIF-95 foam. (d) CO_2 adsorption isotherms for the as-synthesized ZIF-95 foam at 273 K.

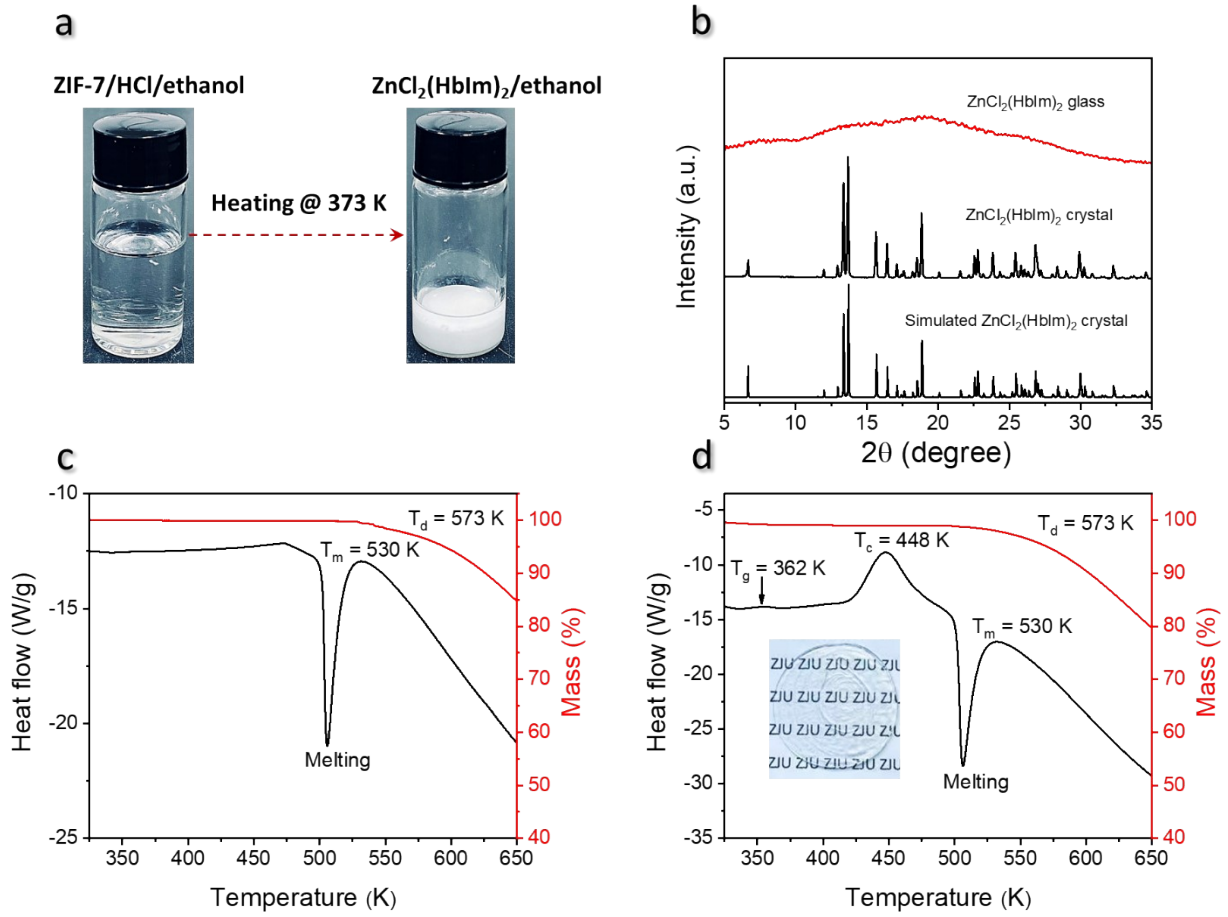

Fig. S8. (a) Schematic illustration for the preparation of $ZnCl_2(HbIm)_2$ crystal. (b) XRD patterns of the as-synthesized $ZnCl_2(HbIm)_2$ crystal and $ZnCl_2(HbIm)_2$ glass. DSC/TGA traces of the as-synthesized (c) $ZnCl_2(HbIm)_2$ crystal and (d) $ZnCl_2(HbIm)_2$ glass. The inset of d is the photograph of the melt-quenched $ZnCl_2(HbIm)_2$ glass.

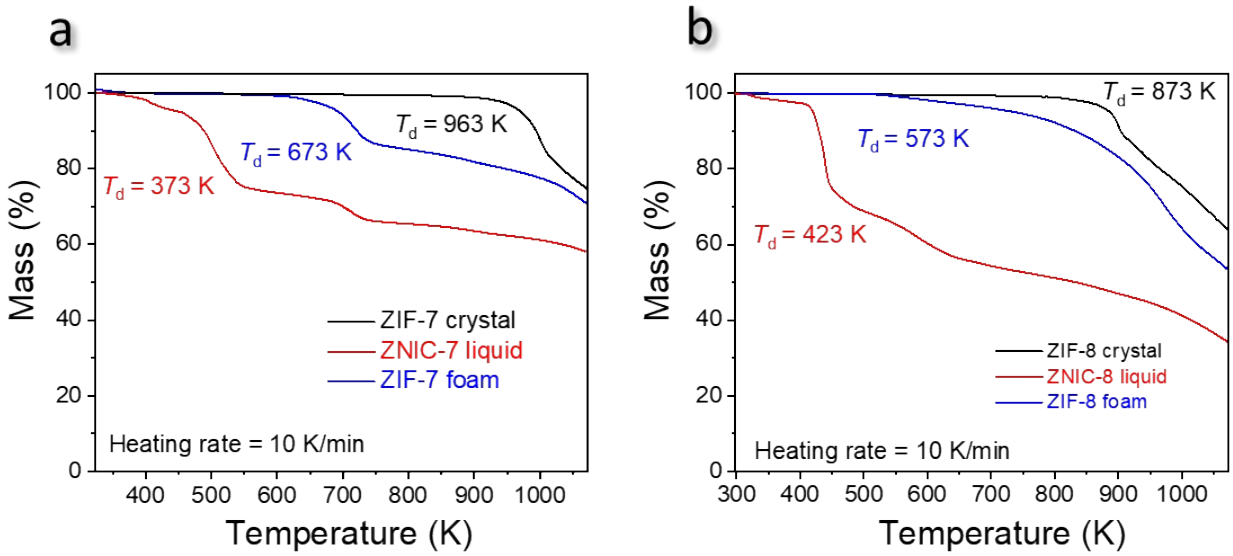

Fig. S9. TGA traces of the as-synthesized (a) ZIF-8 crystal, ZNIC-8 liquid, and ZIF-8 foam and (b) ZIF-8 crystal, ZNIC-8 liquid, and ZIF-8 foam.

Table S1. Density values of the as-synthesized ZIF crystals and ZIF foams measured by Archimedes method.

Sample	Mass in air (g)	Mass in ethanol (g)	Density (gcm^{-3})	Mass in air (g)	Mass in ethanol (g)	Density (gcm^{-3})	Mass in air (g)	Mass in ethanol (g)	Density (gcm^{-3})	Average density (gcm^{-3})
ZIF-7 crystal	0.2966	0.1512	1.609	0.3124	0.1599	1.616	0.2684	0.1357	1.595	1.607
ZIF-7 foam	0.3381	0.1519	1.432	0.3564	0.1597	1.429	0.3121	0.1412	1.440	1.434
ZIF-8 crystal	0.2241	0.0662	1.119	0.2534	0.0719	1.101	0.1934	0.0572	1.120	1.113
ZIF-8 foam	0.2771	0.0456	0.944	0.2995	0.0502	0.947	0.2562	0.0412	0.940	0.944

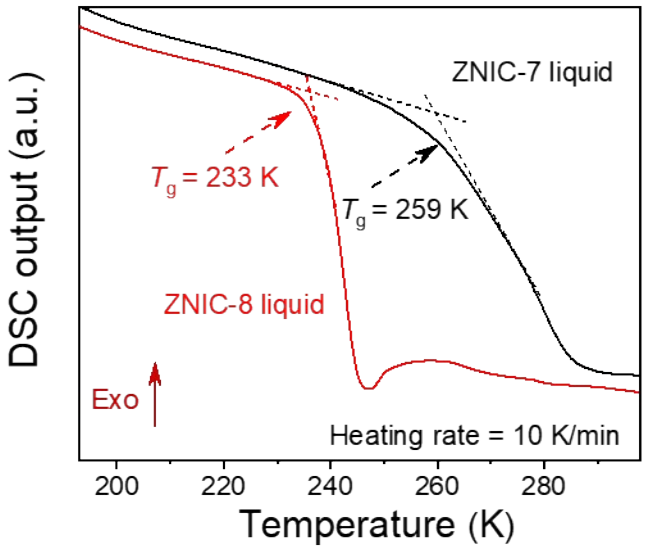

Fig. S10. DSC traces of the as-synthesized ZNIC liquids.

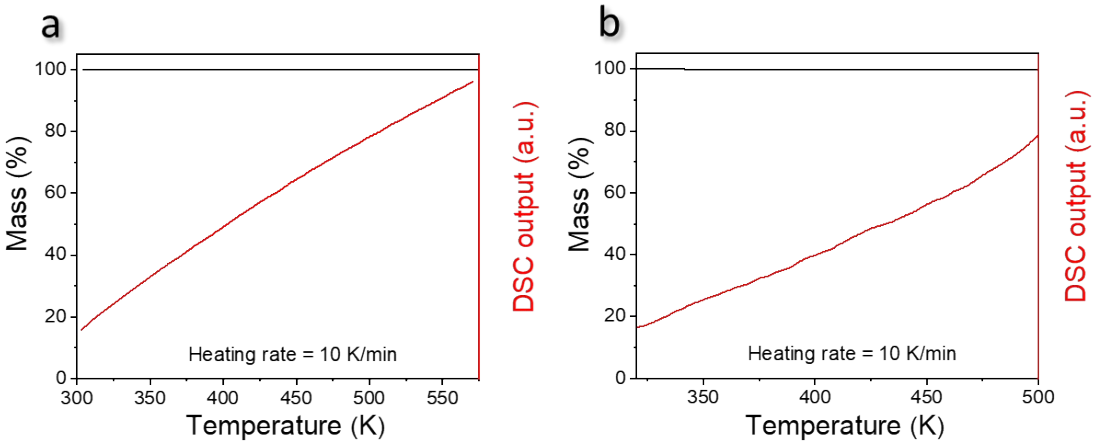

Fig. S11. DSC/TGA traces of the as-synthesized (a) ZIF-7 foam and (b) ZIF-8 foam.

I. Structral differences between ZIF crystals, ZNIC liquids, and ZIF foams:

The FTIR spectra of both the as-synthesized ZIF-7 and ZIF-8 crystals display the characteristic vibration bands of ZIF-7 and ZIF-8.[1,2,3] The FTIR vibration bands of ZNIC liquids are different from those of their parent ZIFs in terms of band position and intensity. The ZNIC liquids exhibit three prominent bands at 1385 cm^{-1}, 3270 cm^{-1}, and 3500 cm^{-1}, which are attributed to the vibrations of the N-O, N-H, and O-H bonds, respectively. This observation suggests the existence of water within the ZNIC liquids and indicates the protonation of organic linkers during the solvation process of ZIFs.[4,5,6] After thermal treatment of ZNIC liquids, the N-O, N-H, and O-H bands disappear in the FTIR spectra of the as-synthesized ZIF foams (Figs. S12 and S13), indicating the deprotonation of organic linkers and the complete removal of nitrates and water. Interestingly, the vibration bands observed in the FTIR spectra of the as-synthesized ZIF foams like glasses are broader than those of the parent ZIF crystals (Figs. S14 and S15). But their band positions are closer to those of the parent ZIF crystals. A new vibration band is observed in the ZIF-7 foam spectrum at 1518 cm^{-1}, being assigned to the vibration of C=O bonds.[7] The FTIR results confirm that the as-synthesized ZIF crystals and their corresponding foams possess an identical molecular structure.[8] In addition, the bIm linkers in ZIF-7 foam were oxidized during thermal treatment, while the mIm linkers remain unchanged. This is also confirmed by the solution ^{1}H-NMR measurements (Figs. S16 and S17), in which the as-synthesized ZIF-8 crystal and ZIF-8 foam demonstrate typical proton resonances of mIm linkers. Furthermore, the H_2/H_5 proton resonance peaks of bIm disappear in the solution ^{1}H-NMR spectrum of ZIF-7 foam. In contrast, the proton integration values for H_1 and H_3/H_4 are 1 and 2, respectively. This observation and FTIR results indicate that the C_3/C_6 atoms in the bIm of ZIF-7 foam are oxidized during the heat treatment of

ZNIC-7 liquid at 573 K. The protonation and deprotonation of organic linkers are further confirmed by the ^{1}H CPMAS-NMR measurements (Fig. S18). A broad proton resonance peak associated with H-N bonds (@ 11.87 ppm) is detected only for ZNIC liquids. However, this peak diminishes notably in the spectra of both ZIF crystals and ZIF foams. The deprotonation of organic linkers implies the formation of Zn-bIm/mIm-Zn coordination bonds (i.e., the formation of ZIF structure). Moreover, the ^{1}H and ^{13}C CPMAS-NMR measurements (Figs. S18-S20) further confirm a high degree of structural disorder in the foam samples. This is evidenced by the broader resonance peaks observed in the foam samples compared to their respective ZIF crystals. Essentially, this signifies that the distribution of bond lengths and angles of the organic linkers is broader in the foam state than in the crystal form. For example, the proton resonance peak of mIm broadens following the transition from the ZIF-8 crystal into the ZNIC-8 liquid and becomes even broader in the case of the ZIF-8 foam. A similar trend is observed for ZIF-7 structure, yet the width of the proton resonance peaks diminishes subsequent to the removal of water and nitrates owing to the oxidation of bIm. Just like the ^{1}H CPMAS-NMR spectra, the ^{13}C CPMAS-NMR spectra of the as-synthesized ZIF crystals match well with those of their ZIF foams, yet the resonance bands in the spectra of foams are considerably broader compared to the crystals (Figs. S19 and S20).[9] Unlike the ^{13}C CPMAS−NMR spectra of both ZIF crystals and ZIF foams, interestingly, the ^{13}C CPMAS−NMR spectra of the as-synthesized ZNIC-7 and ZNIC-8 liquids (Figs. S19 and S20) exhibit additional broad resonance peaks around 131 ppm/138 ppm and 118 ppm, respectively. These results imply that the transformation of bIm/mIm into Hbim/HmIm during ZIF solvation results in the formation of the independent Hbim/HmIm, subsequently revert to the dependent bIm/mIm upon heat treatment.[4,5,10,11] The observed peak broadening in the NMR spectra of foam

samples implies that the structure of the ZIF crystals is strongly perturbed upon alcohol/acid attack.[12,13,14] This observation also indicates a high degree of distortion in C-H and C-C bonds of organic linkers upon vitrification. The similar characteristics in the FTIR and NMR spectra of both the ZIF foams and the ZIF crystals imply the preservation of organic linkers and molecular structure of ZIFs after the two-step perturbations. This is further confirmed by the ICP-MS measurement and elemental analysis (Table S2). Elemental analysis shows a negligible difference between crystalline and perturbed ZIF-8, whereas the composition of the ZIF-7 foam is slightly different from that of ZIF-7 crystal because of the oxidation of bIm during heat treatment. The X-ray-PDF D(*r*) data of both the ZIF-7 crystal and its corresponding foam (Fig. S21) suggest that the correlations between Zn and bIm remain intact in the ZIF-7 foam, since the observed C-N, Zn-N, Zn-C, and Zn-Zn correlations in the foam sample are similar to those in ZIF-7 crystal.[13,15] This observation indicates that the ZIF foam synthesized by the structural perturbation approach possesses similar short-range order correlations as the parent crystalline counterpart. The increase in the intensity of the correlation peak at 1.32 Å suggests a contribution from C-O bonds, confirming the oxidation of bIm. The D(*r*) data of the ZNIC-7 liquid (Fig. S21) endorses that the correlations between Zn and NO_3/HbIm are formed in the ZNIC liquid; where the C-N/N-O, Zn-N/Zn-O/O-O, and Zn–C correlations are clearly observed at 1.34 Å, 2.04 Å/4.12 Å, and 2.97 Å, respectively. While, the Zn–Zn correlation fades in in the spectrum of ZNIC-7 liquid, indicating the conversion of coordination bonded ZIF-7 network (i.e., Zn-bIm-Zn) into the hydrogen bonded ZNIC-7 network (i.e., Hbim-Zn-NO_3). Observing the SEM images (Figs. S22 and S23), it's evident that the ZIF-7 and ZIF-8 crystals showcase layered and polyhedral geometries, respectively. In contrast, both ZNIC liquids and ZIF foams appear as particles with irregular geometry. From these

observations, we infer that the vitrification of layered ZIF-7 crystals leads to the transformation of the network structure from 2D to shapeless network. This transformation is also confirmed by TEM measurements (Figs. S24 and S25). In addition, the SAED patterns of the as-synthesized ZIF foams do not show any interfered fringes, implying the amorphous nature of the ZIFs (insets of Figs. S24 and S25). Moreover, the TEM/EDS mappings of both the as-synthesized ZIF crystals and their respective foams (Figs. S26-S29) show that the Zn, C, and N elements are distributed homogeneously in ZIF networks. But it should be noted that, besides Zn/C/N, oxygen is also present in ZIF-7 foam due to the oxidation of bIm linkers (Fig. S27). These results are in line with the FTIR, NMR and elemental analyses.

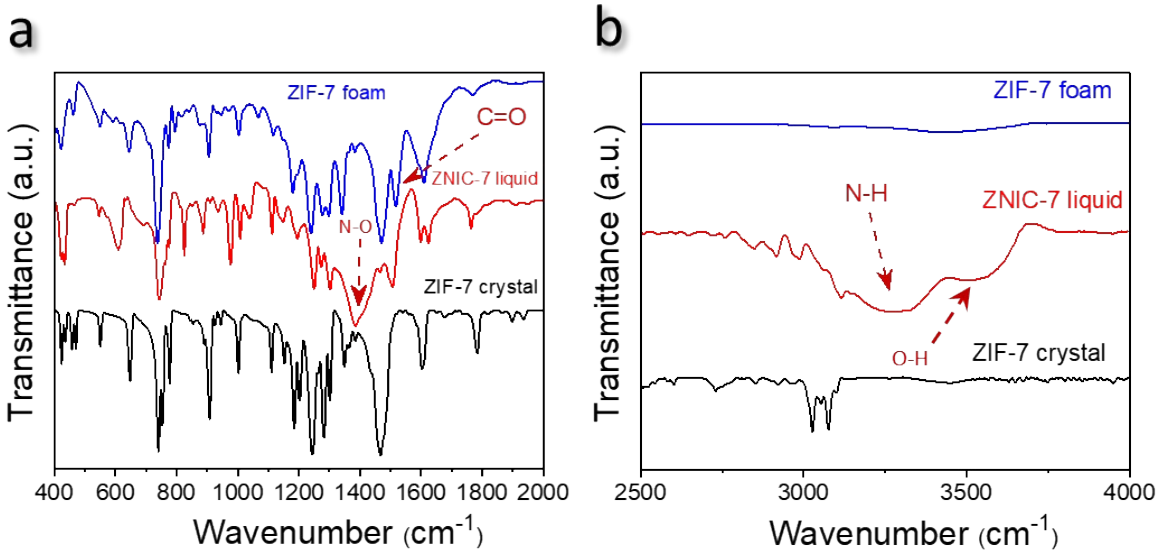

Fig. S12. FTIR spectra of the as-synthesized ZIF-7 crystal, ZNIC-7 liquid, and ZIF-7 foam at RT in the wavenumber range of (a) 400 – 2000 cm^{-1} and (b) 2500 – 4000 cm^{-1}.

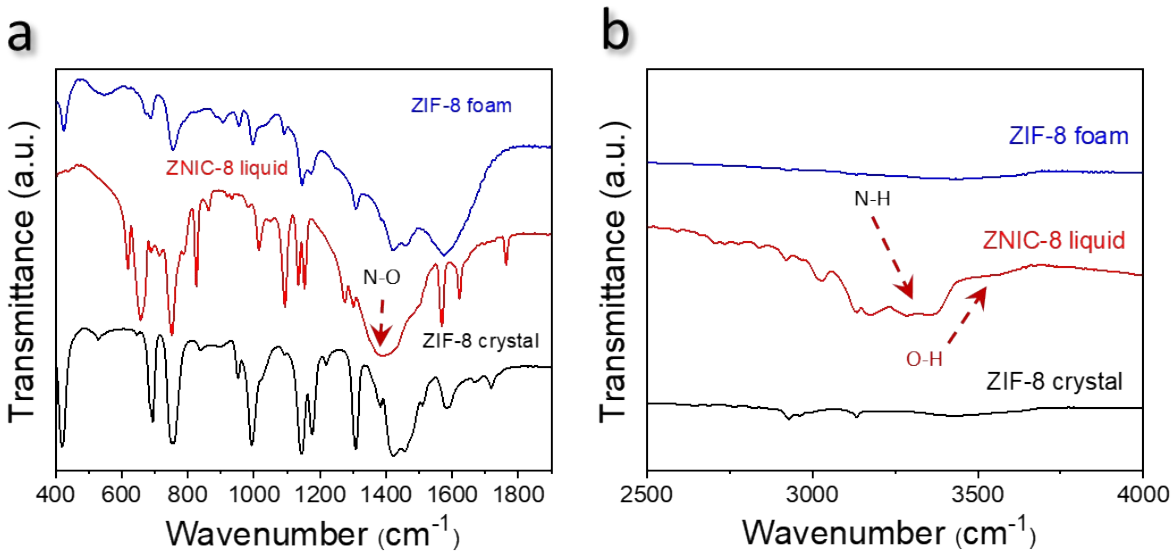

Fig. S13. FTIR spectra of the as-synthesized ZIF-8 crystal, ZNIC-8 liquid, and ZIF-8 foam at RT in the wavenumber range of (a) 400 – 2000 cm^{-1} and (b) 2500 – 4000 cm^{-1}.

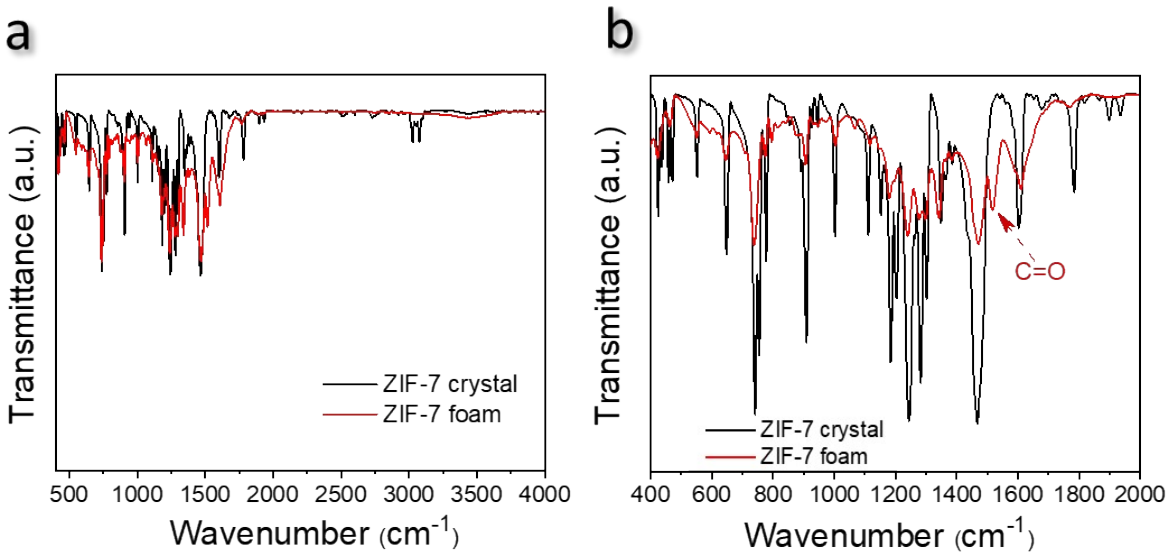

Fig. S14. FTIR spectra of the as-synthesized ZIF-7 crystal and ZIF-7 foam at RT in the wavenumber range of (a) 400 – 4000 cm^{-1} and (b) 400 – 2000 cm^{-1}.

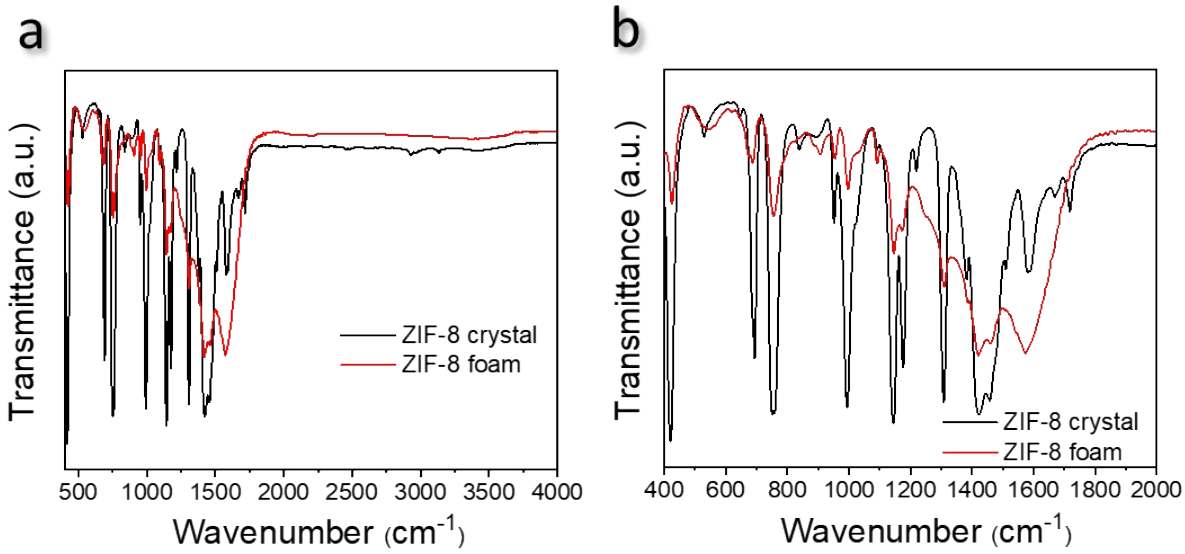

Fig. S15. FTIR spectra of the as-synthesized ZIF-8 crystal and ZIF-8 foam at RT in the wavenumber range of (a) 400 – 4000 cm^{-1} and (b) 400 – 2000 cm^{-1}.

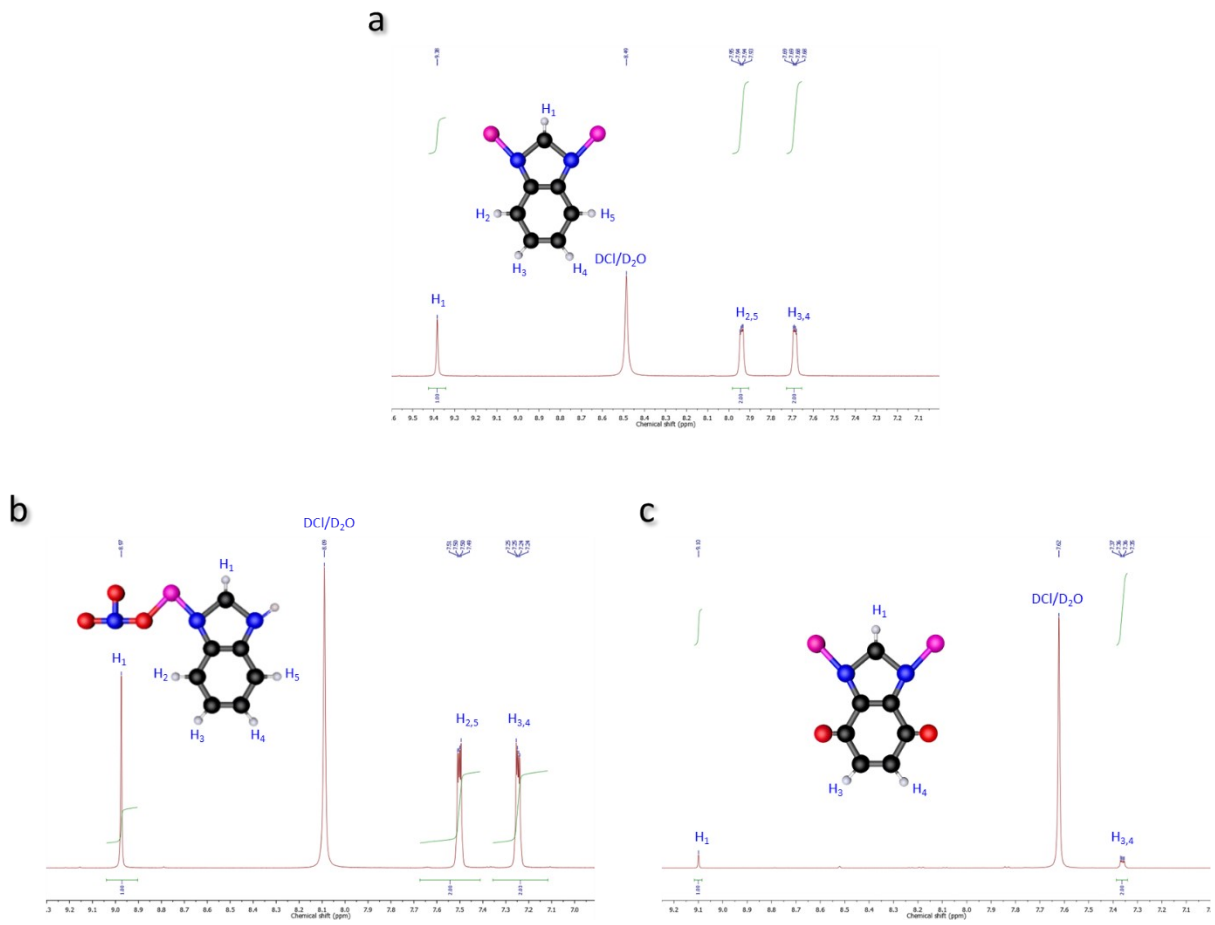

Fig. S16. Solution ^{1}H-NMR spectra of the as-synthesized (a) ZIF-7 crystal, (b) ZNIC-7 liquid, and (c) ZIF-7 foam at RT, including the proton integration values (green numbers) and the number of protons in each linker (blue numbers). The inset is the molecular structure of ZIF-7 before (left) and after (right) vitrification.

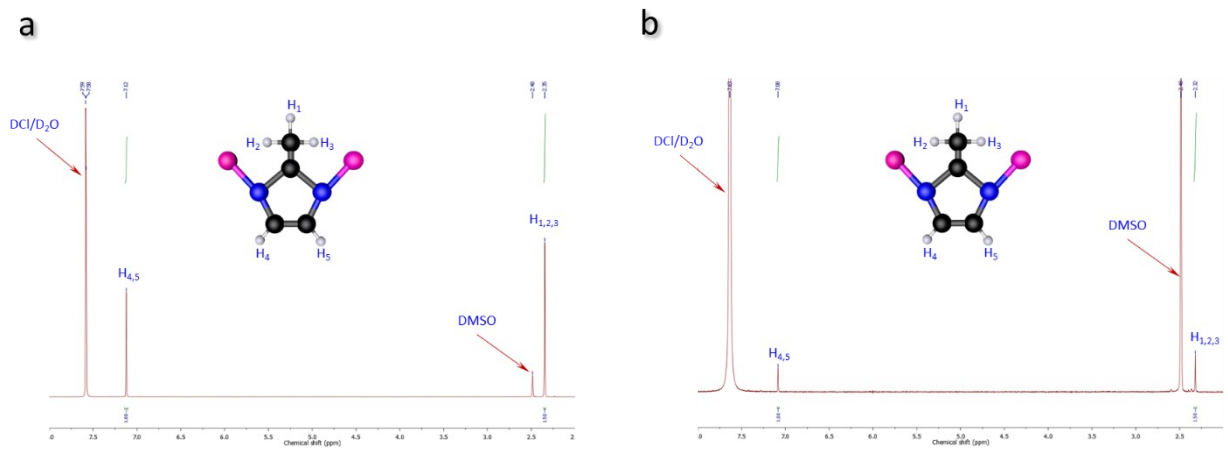

Fig. S17. Solution ^{1}H-NMR spectra of the as-synthesized (a) ZIF-8 crystal and (b) ZIF-8 foam at RT, including the proton integration values (green numbers) and the number of protons in each linker (blue numbers). The inset is the molecular structure of ZIF-8 before (left) and after (right) vitrification.

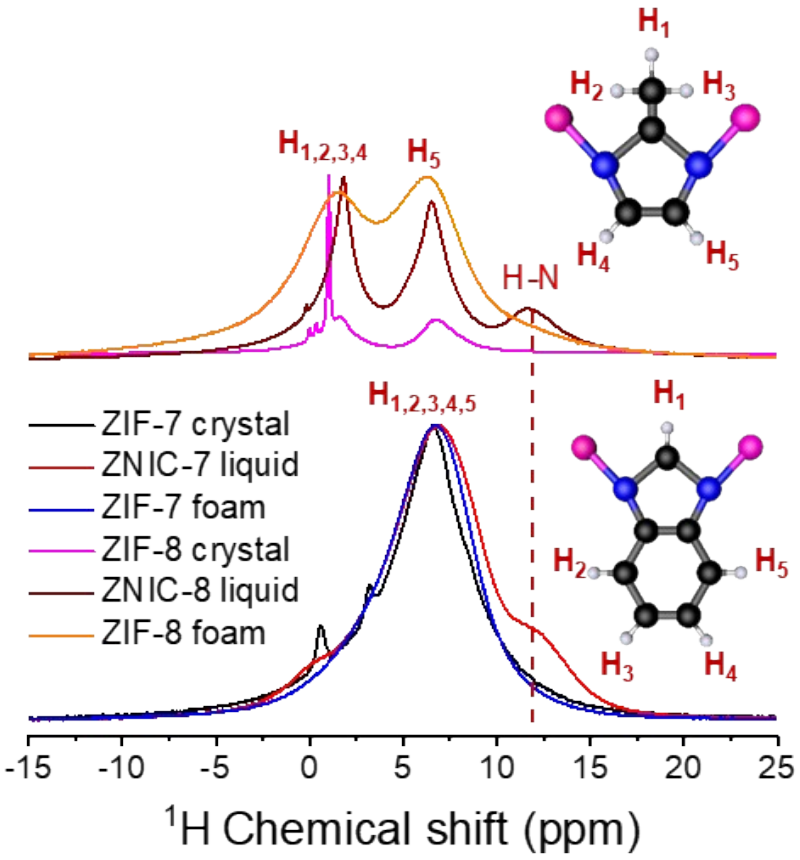

Fig. S18. ^{1}H CPMAS-NMR spectra of the as-synthesized ZIF-7 crystal, ZNIC-7 liquid, ZIF-7 foam, ZIF-8 crystal, ZNIC-8 liquid, and ZIF-8 foam at RT. The inset is the molecular structure of ZIF-8 (up) and ZIF-7 (down).

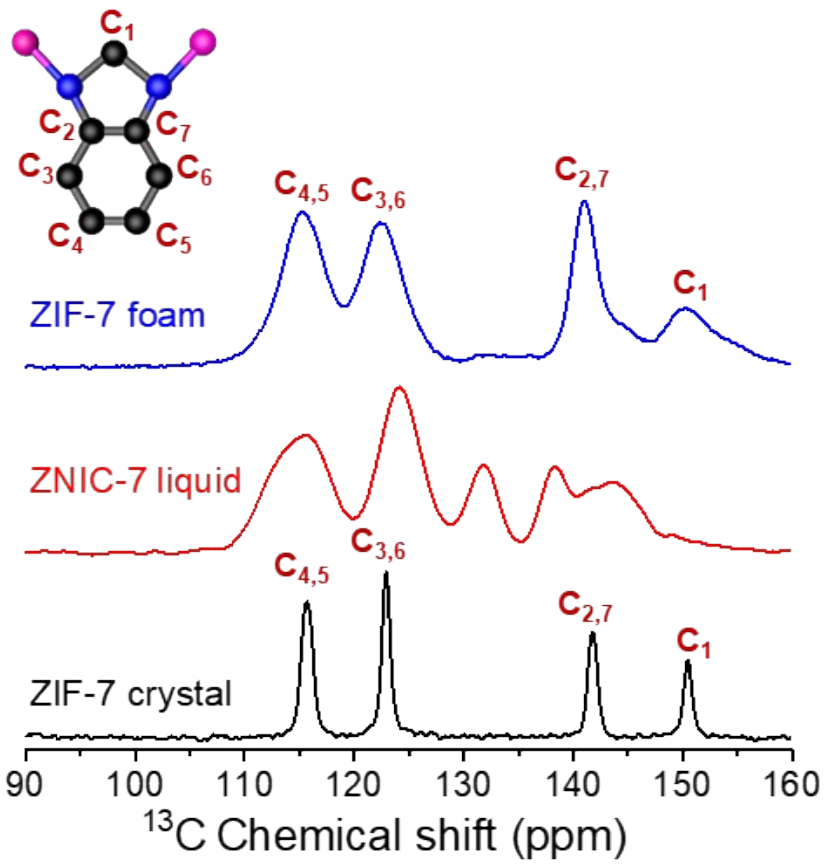

Fig. S19. ^{13}C CPMAS-NMR spectra of the as-synthesized ZIF-7 crystal, ZNIC-7 liquid, and ZIF-7 foam at RT. The inset is the molecular structure of ZIF-7.

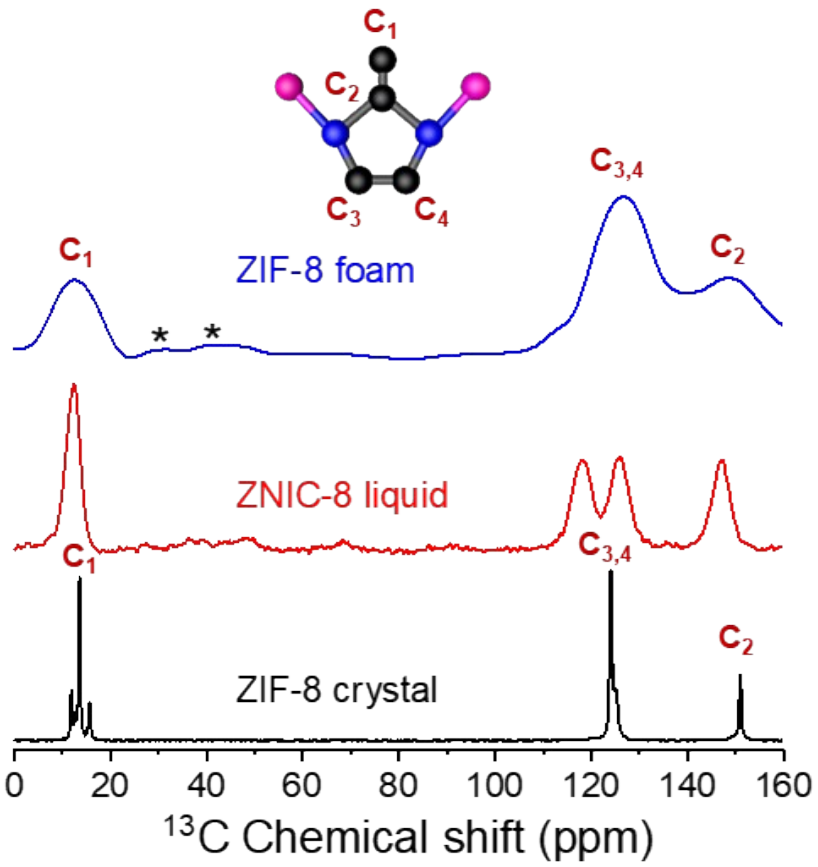

Fig. S20. ^{13}C CPMAS-NMR spectra of the as-synthesized ZIF-8 crystal, ZNIC-8 liquid, and ZIF-8 foam at RT. Spinning sidebands are marked with asterisks. The inset is the molecular structure of ZIF-8.

Table S2. Elemental analysis of the as-synthesized ZIF-7 crystal, ZIF-7 foam, ZIF-8 crystal, and ZIF-8 foam by ICP-MS and CHNO measurements.

Sample	Calculated (wt%)					Measured (wt%)				
	Zn	N	C	H	O	Zn	N	C	H	O
ZIF-7 crystal $Zn(C_7N_2H_5)_2$	21.83	18.69	56.12	3.36	-	21.61	18.55	55.95	3.35	<0.01
ZIF-7 foam $Zn(C_7N_2H_3O_2)_2$	18.18	15.58	46.76	1.68	17.80	18.37	15.44	46.34	1.61	17.75
ZIF-8 crystal $Zn(C_4N_2H_5)_2$	28.73	24.62	42.22	4.43	-	28.62	24.54	42.19	4.43	<0.01
ZIF-8 foam $Zn(C_4N_2H_5)_2$	28.73	24.62	42.22	4.43	-	29.96	23.98	41.13	4.21	<0.01

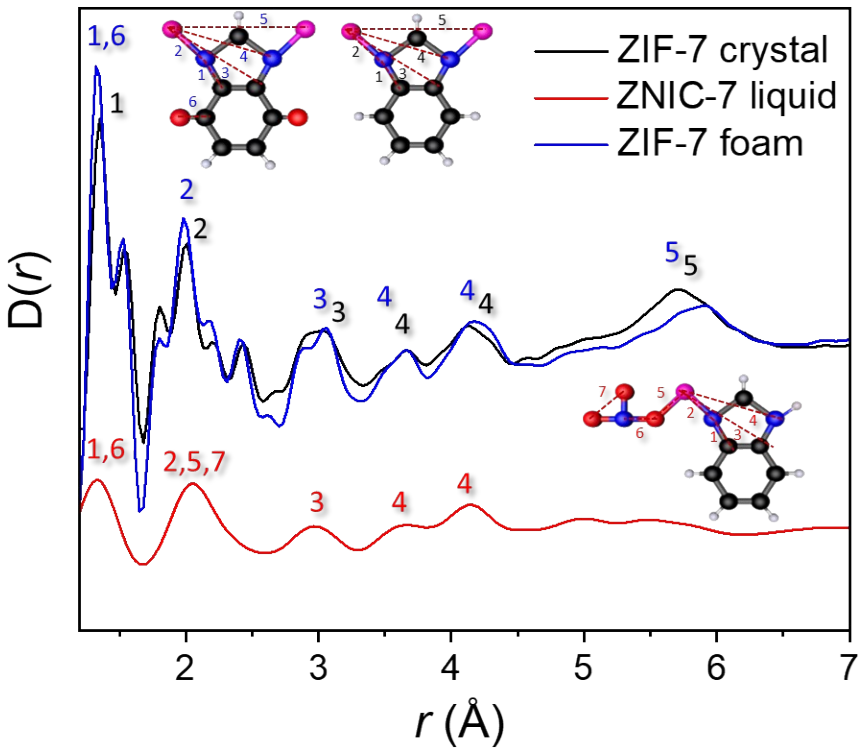

Fig. S21. X-ray PDF data of the as-synthesized ZIF-7 crystal, ZNIC liquid, and ZIF-7 foam.

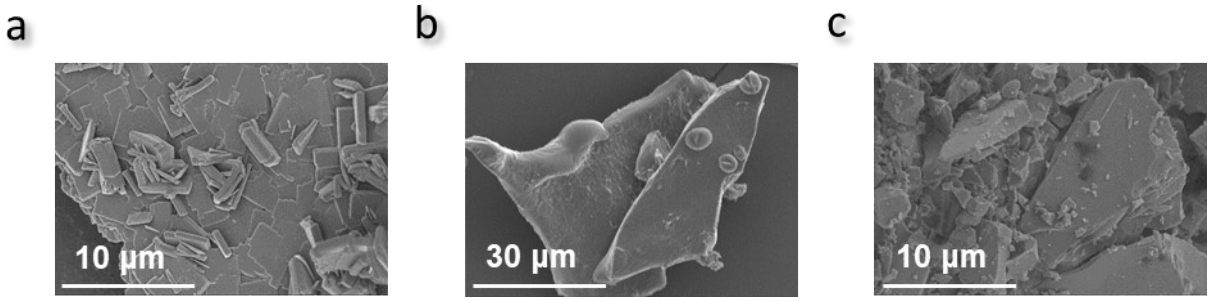

Fig. S22. SEM images of the as-synthesized (a) ZIF-7 crystal, (b) ZNIC-7 liquid, and (c) ZIF-7 foam at RT.

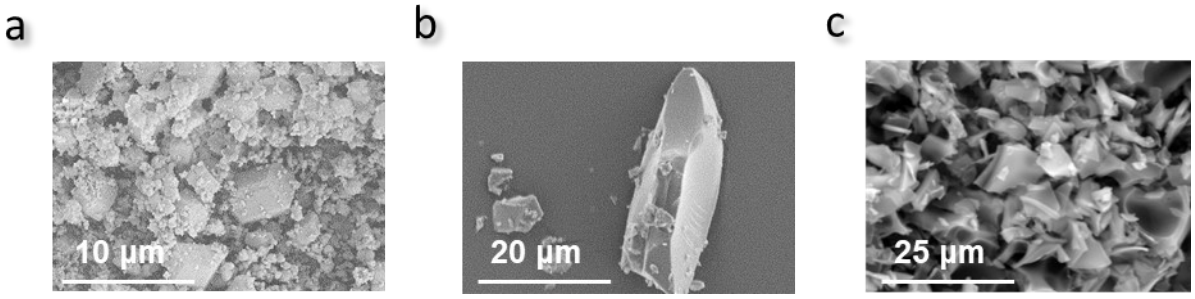

Fig. S23. SEM images of the as-synthesized (a) ZIF-8 crystal, (b) ZNIC-8 liquid, and (c) ZIF-8 foam at RT.

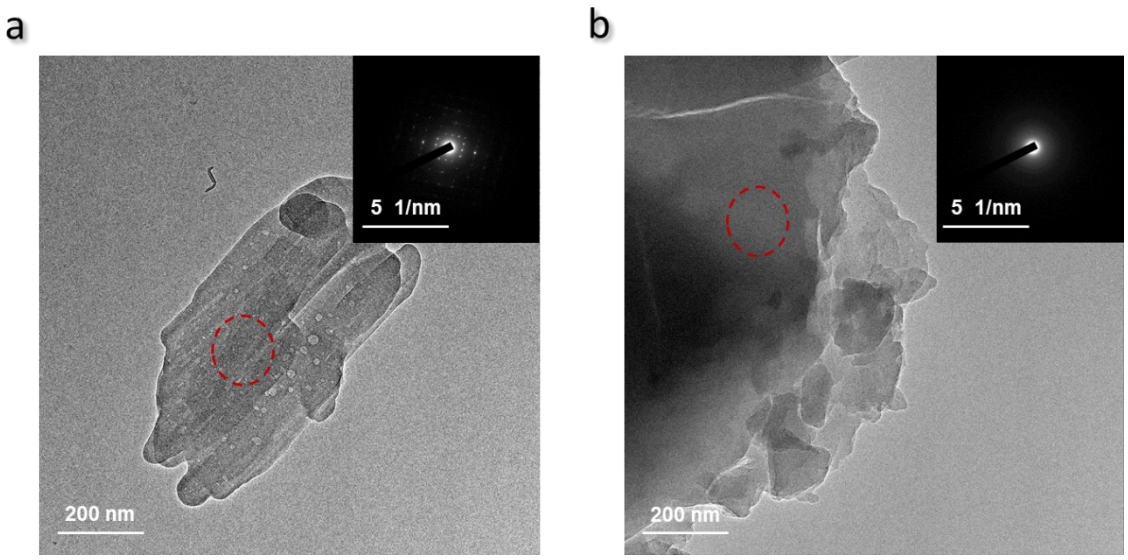

Fig. S24. TEM images of the as-synthesized (a) ZIF-7 crystal and (b) ZIF-7 foam at RT. The inset of a and b are the SAED patterns of areas circled in red.

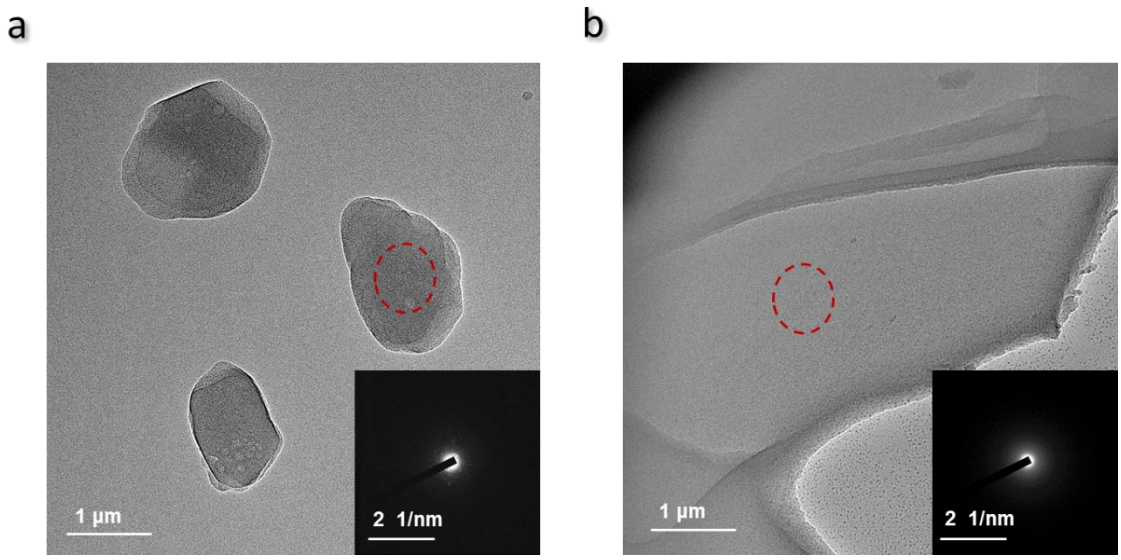

Fig. S25. TEM images of the as-synthesized (a) ZIF-8 crystal and (b) ZIF-8 foam at RT. The inset of a and b are the SAED patterns of areas circled in red.

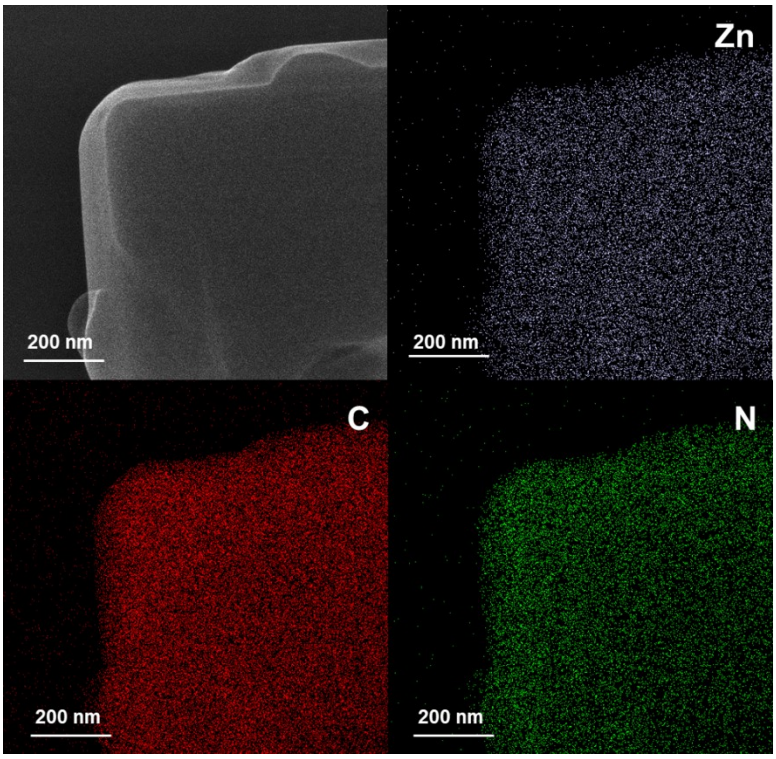

Fig. S26. TEM/EDS mappings of the as-synthesized ZIF-7 crystal at RT.

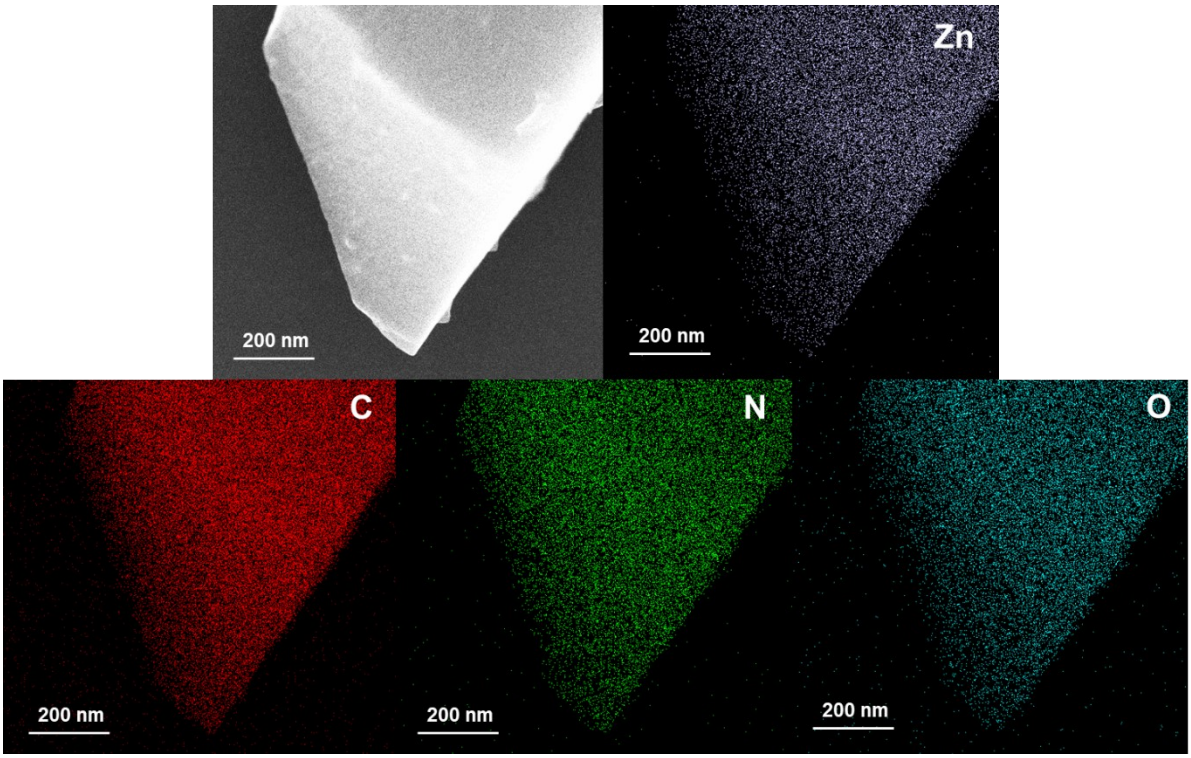

Fig. S27. TEM/EDS mappings of the as-synthesized ZIF-7 foam at RT.

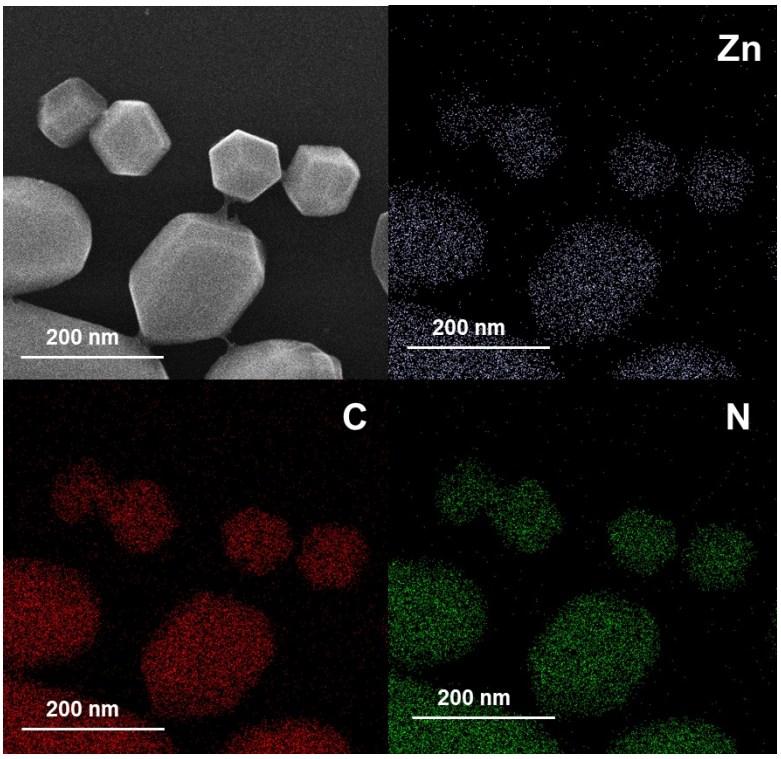

Fig. S28. TEM/EDS mappings of the as-synthesized ZIF-8 crystal at RT.

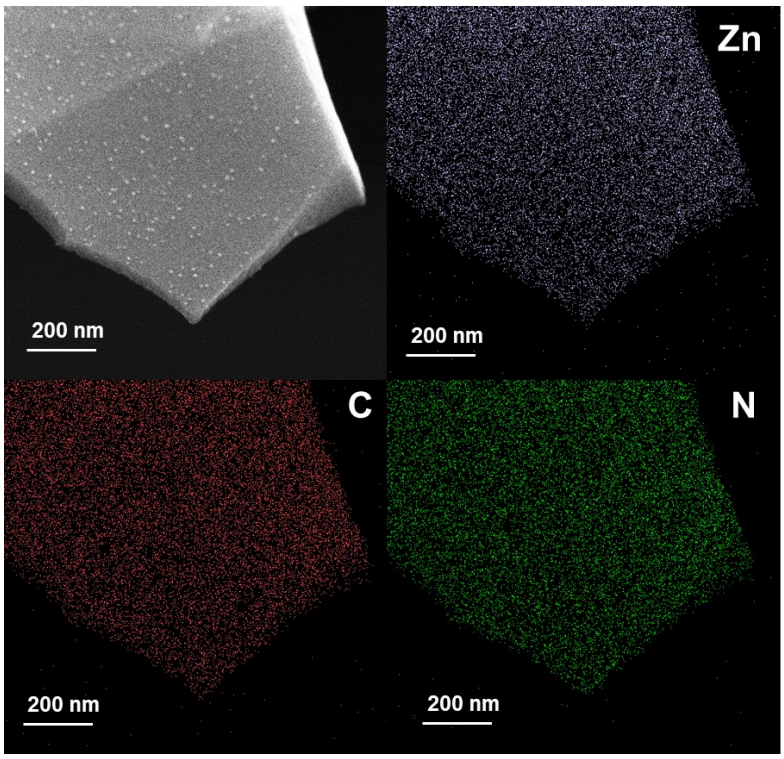

4

Fig. S29. TEM/EDS mappings of the as-synthesized ZIF-8 foam at RT.

II. Gas adsorption of ZIF crystals and ZIF foams:

Based on the BET model and DFT calculations for gas adsorption-desorption isotherms (Table S4), it is found that the N_2-BET surface area/total pore volume for ZIF-7 and ZIF-8 foams are 19 $m^2 g^{-1}$/0.012 $cm^3 g^{-1}$ and 41 $m^2 g^{-1}$/0.074 $cm^3 g^{-1}$, respectively. On the other hand, the DFT calculations for the CO_2 gas adsorption-desorption (@ 273 K) suggest that the total pore volume in ZIF-7/ZIF-8 increases/decreases by 7.50/1.94 times after foam formation, respectively. The CO_2-DFT surface area/total pore volume (@ 273 K) are found to be 7 $m^2 g^{-1}$ / 0.002 $cm^3 g^{-1}$, 60 $m^2 g^{-1}$ / 0.015 $cm^3 g^{-1}$, 133 $m^2 g^{-1}$ / 0.031 $cm^3 g^{-1}$, and 62 $m^2 g^{-1}$ / 0.016 $cm^3 g^{-1}$ for ZIF-7 crystal, ZIF-7 foam, ZIF-8 crystal, and ZIF-8 foam, respectively. In comparison with the melt-quenched ZIF glasses (e.g., ZIF-4, ZIF-62, ZIF-76, ZIF-8/IL, and ZIF-UC, and MUV-24),[2,12,16,18-22] both ZIF-7 and ZIF-8 foams synthesized by structural perturbation approach exhibit unique gas adsorption capabilities (Table S4). For example, the melt-quenched ZIF-76 and ZIF-UC glasses can only adsorb CO_2 gas at 273 K (30 $cm^3 g^{-1}$ for ZIF-76 glass and 18-42 $cm^3 g^{-1}$ for ZIF-UC glasses at 100 kPa),[12,21] and do not adsorb the larger N_2 gas molecules. In addition, the melt-quenched ZIF-4 and MUV-24 glasses do not demonstrate any signs for gas adsorption,[20,22] despite the formation of pores in ZIF-4 glass.[23] Similar to ZIF-76 and ZIF-UC glasses, ZIF-62 glass blocks the N_2 gas diffusion in glass, and hence exhibiting adsorption only for smaller gas molecules such as O_2, H_2, and CO_2.[19] It was reported that the porosity of ZIF-62 glass could be improved through the preparation of glass foam, allowing ZIF-62 glass to adsorb a minor amount of N_2 gas (~ 3 $cm^3 g^{-1}$ @ 77 K and 100 kPa) and CO_2 gas (~ 30 $cm^3 g^{-1}$ @ 273 K and 100 kPa).[16] Based on the N_2-BET model, the total pore volume and BET surface area of ZIF-62 glass foam are 0.005 $cm^3 g^{-1}$ and 2.83 $m^2 g^{-1}$, which are relatively low. In addition, the non-pure ZIF-8/IL glass exhibits adsorption for CO_2 gas (10-15 $cm^3 g^{-1}$) and

N_2 gas (5-10 $cm^3\ g^{-1}$) with a total pore volume (0.001-0.003 $cm^3\ g^{-1}$) and BET surface area (16-17 $m^2\ g^{-1}$).[2] Inspiringly, the as-synthesized ZIF-7 and ZIF-8 foams by structural perturbation approach demonstrate noteworthy adsorption capacities for various gases, including N_2. This stands in contrast to several melt-quenched ZIF glasses, which are unable to adsorb N_2 gas. These two ZIF foams obtained from this work record relatively high N_2 gas uptake of 7.50 $cm^3\ g^{-1}$ and 47.94 $cm^3\ g^{-1}$, respectively. Moreover, compared with the melt-quenched ZIF glasses, both ZIF-7 and ZIF-8 foams display the highest total pore volume (0.012-0.074 $cm^3\ g^{-1}$) and BET surface area (19-41 $m^2\ g^{-1}$) based on the N_2-BET model. Remarkably, we have also observed that the as-synthesized ZIF foam exhibiting a higher gas adsorption capacity than the parent ZIF crystal, as seen in ZIF-7. This phenomenon seems to stem from the enlargement of pore size resulting from foaming.[17] The gas adsorption in melt-quenched ZIF glasses usually demonstrates lower levels compared to their respective ZIF crystals due to the pore collapse occurring upon vitrification.[12,21] Yet, the amorphization process of ZIF-7 crystal induces to a transformation in the network's dimensionality, shifting from 2D to shapeless network. Consequently, this transformation results in an increase of both pore size and gas adsorption capacities.[16,17]

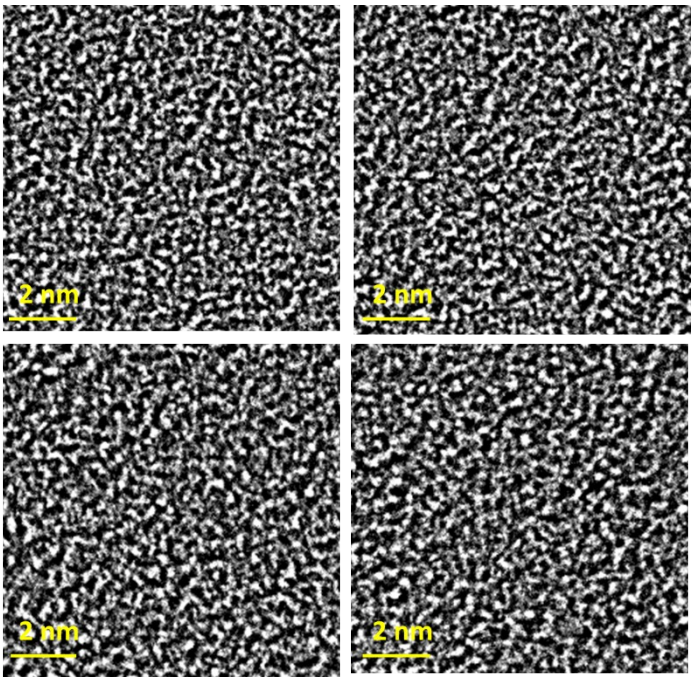

Fig. S30. HR-TEM images of the as-synthesized ZIF-7 foam observed at different areas.

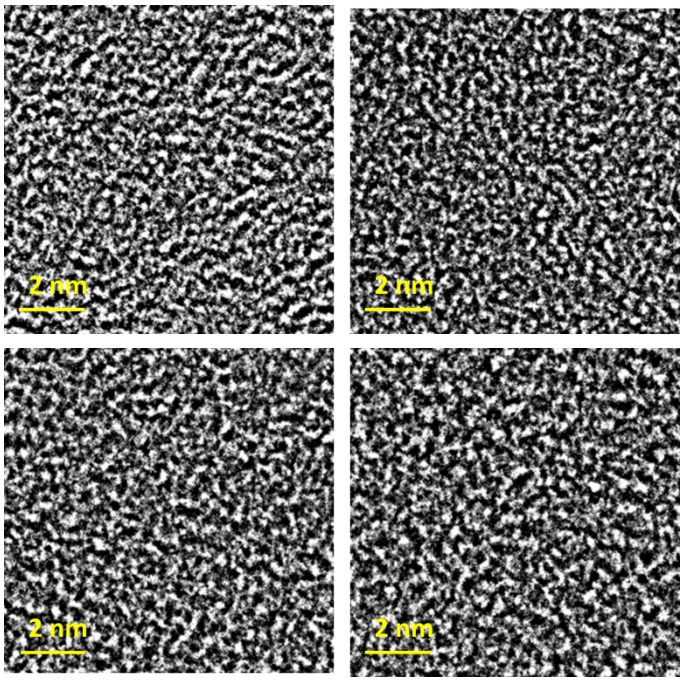

Fig. S31. HR-TEM images of the as-synthesized ZIF-8 foam observed at different areas.

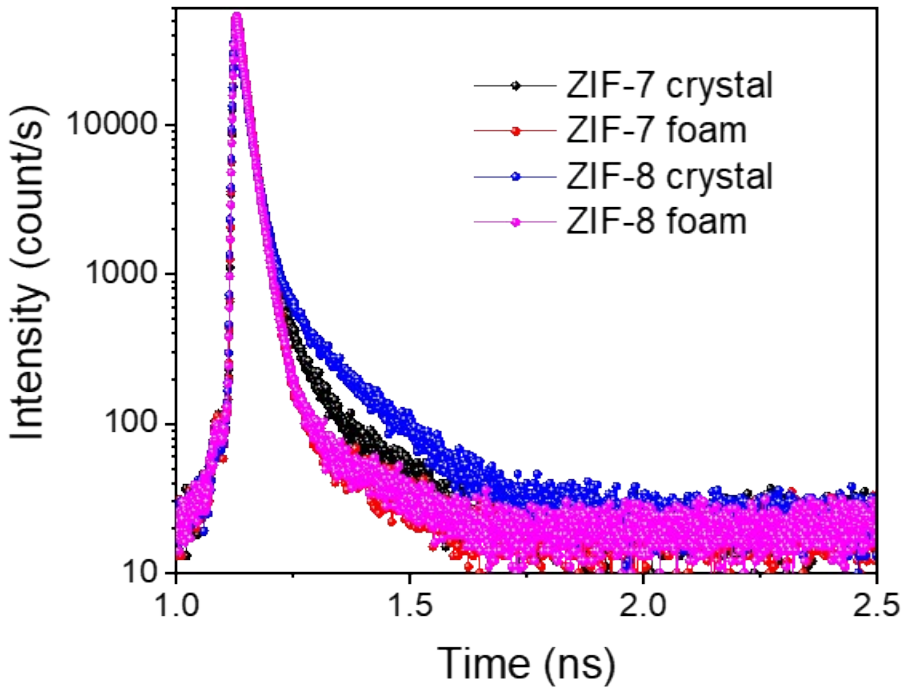

Fig. S32. PALS decay curves of the as-synthesized ZIF-7 crystal, ZIF-7 foam, ZIF-8 crystal, and ZIF-8 foam.

Table S3. PALS results for the as-synthesized ZIF-7 and ZIF-8 crystals and their foams. τ_3, I_3, D_3, V_f, and FFV are the lifetime, intensity, pore diameter, pore volume and fractional free volume at the third part of the decay curves, respectively.

Sample	τ_3(ns)	I_3(%)	D_3(Å)	V_f(Å^3)	FFV(%)
ZIF-7 crystal	2.003	6.1	5.702	97.066	1.080
ZIF-7 foam	2.275	1.9	6.176	123.341	0.430
ZIF-8 crystal	2.517	11.5	6.562	147.943	3.070
ZIF-8 foam	2.295	2.2	6.210	125.389	0.490

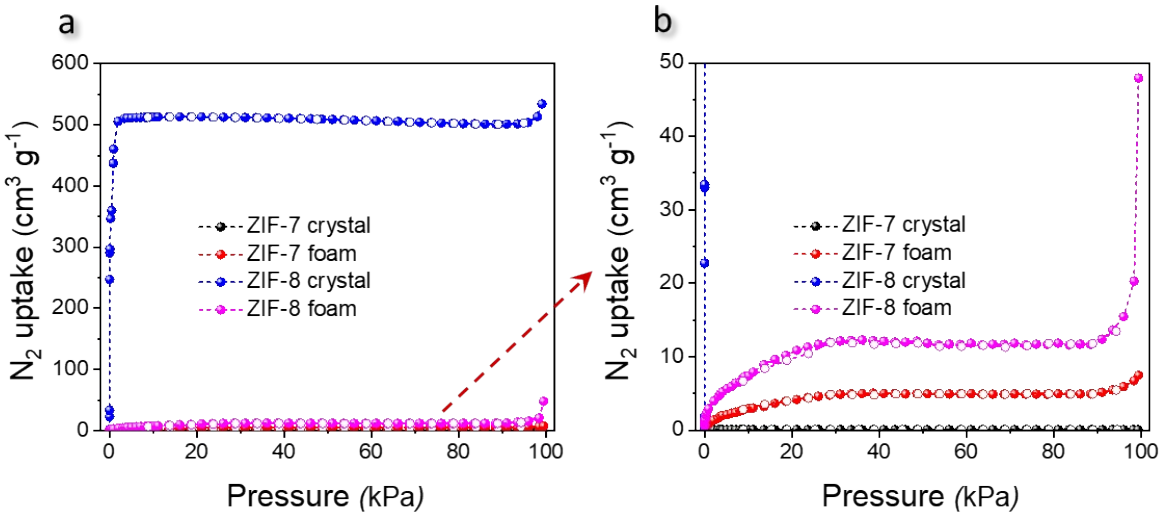

Fig. S33. (a) N_2 adsorption isotherms for the as-synthesized ZIF-7 crystal, ZIF-7 foam, ZIF-8 crystal, and ZIF-8 foam at 77 K. Filled symbols = adsorption, empty symbols = desorption. (b) the magnified N_2 adsorption isotherms of a at the range of N_2 uptake of 0-50 cm^3g^{-1}.

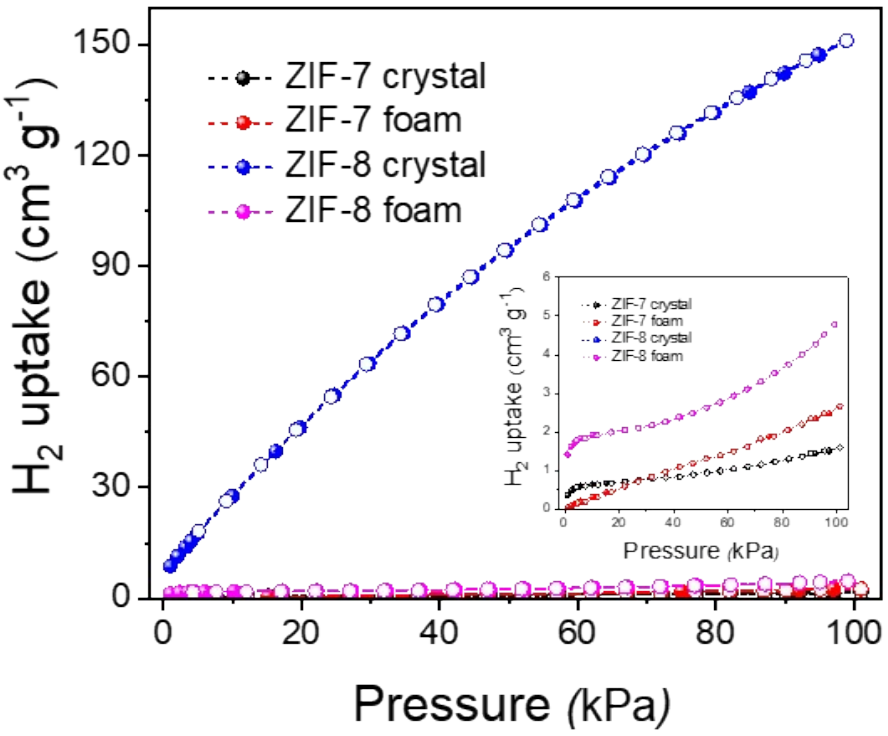

Fig. S34. H_2 adsorption isotherms for the as-synthesized ZIF-7 crystal, ZIF-7 foam, ZIF-8 crystal, and ZIF-8 foam at 77 K. Filled symbols = adsorption, empty symbols = desorption.

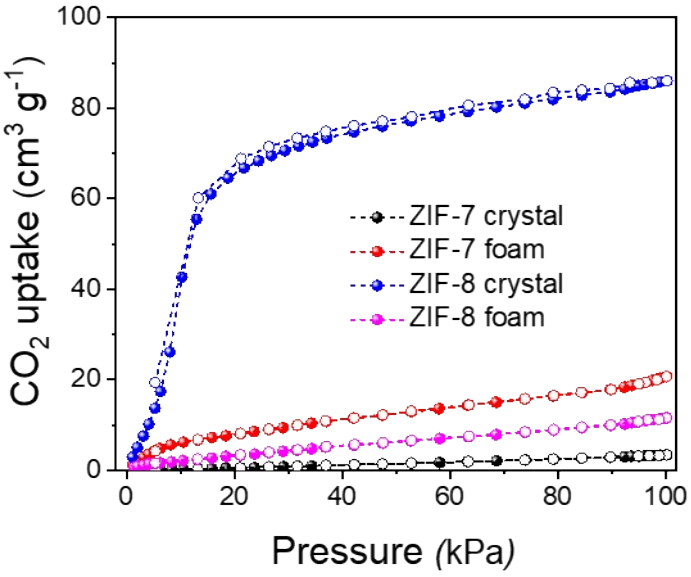

Fig. S35. CO_2 adsorption isotherms for the as-synthesized ZIF-7 crystal, ZIF-7 foam, ZIF-8 crystal, and ZIF-8 foam at 195 K. Filled symbols = adsorption, empty symbols = desorption.

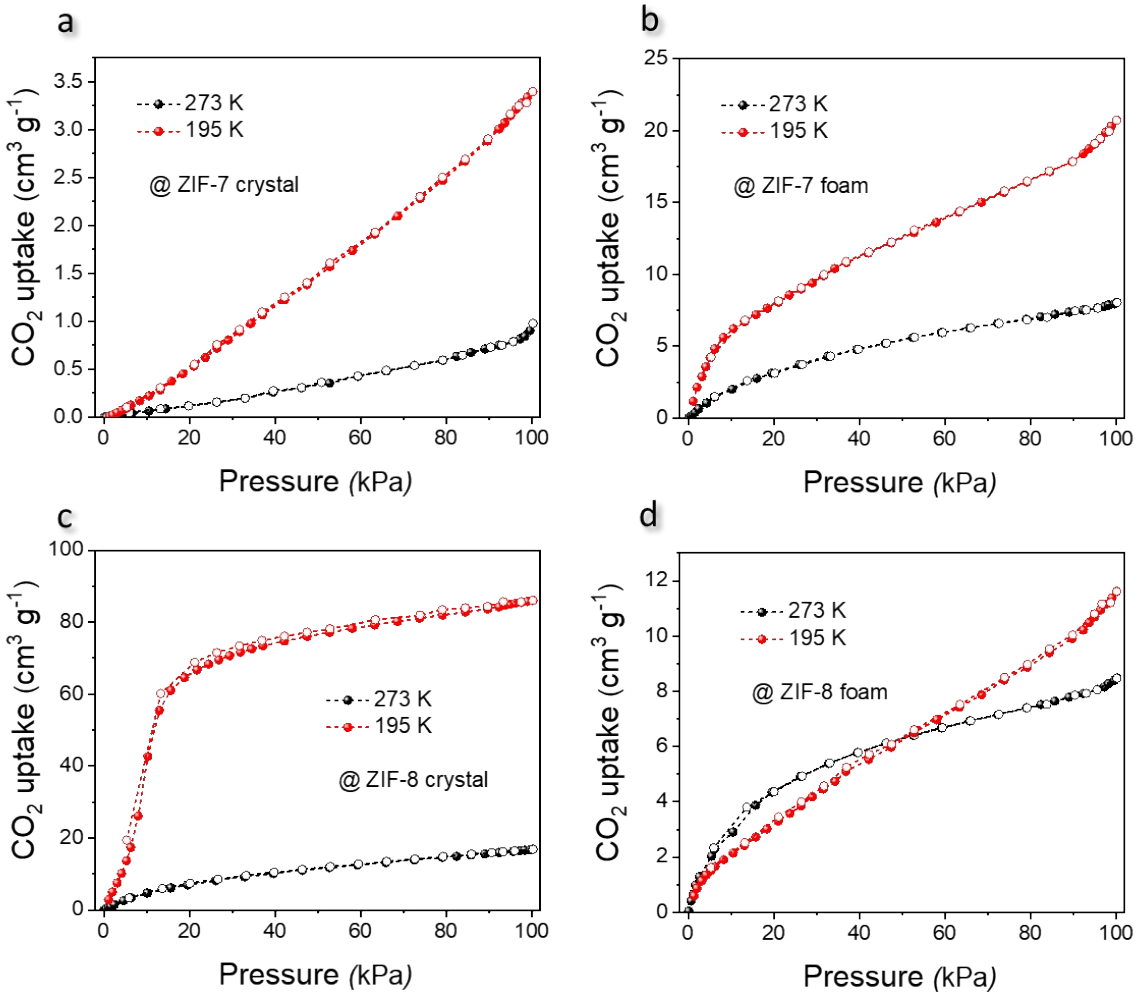

Fig. S36. CO_2 adsorption isotherms for the as-synthesized (a) ZIF-7 crystal, (b) ZIF-7 foam, (c) ZIF-8 crystal, and (d) ZIF-8 foam at 273 K and 195 K. Filled symbols = adsorption, empty symbols = desorption. The CO_2 gas adsorption measurements conducted at lower temperatures (i.e., from 273 K to 195 K) further validate the increased gas adsorption by ZIFs. This suggests the potential for CO_2 diffusion into the pores at lower temperatures, likely facilitated by the transition of CO_2 from a gaseous to a liquid state, contributing to enhanced adsorption. The N_2, H_2, and CO_2 adsorption-desorption isotherms do not show any hysteresis effect, implying that the diffusion limitations are minimized for these gases.

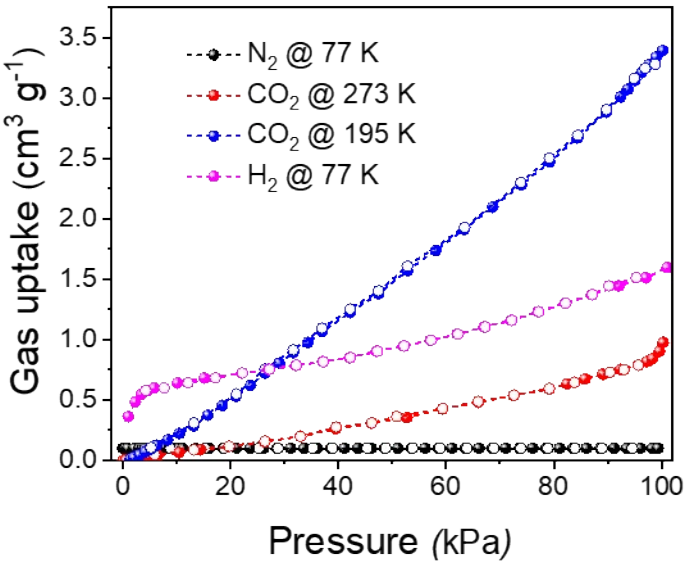

Fig. S37. Gas adsorption isotherms of the as-synthesized ZIF-7 crystals. Filled symbols = adsorption, empty symbols = desorption.

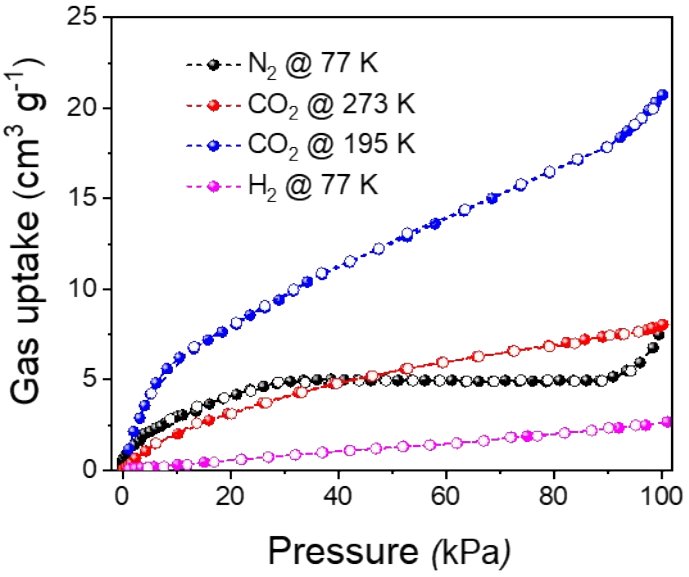

Fig. S38. Gas adsorption isotherms of the as-synthesized ZIF-7 foam. Filled symbols = adsorption, empty symbols = desorption.

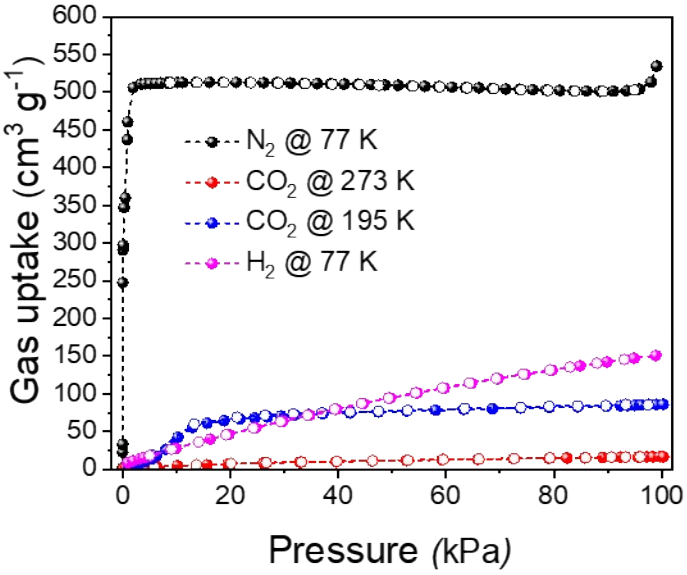

Fig. S39. Gas adsorption isotherms of the as-synthesized ZIF-8 crystals. Filled symbols = adsorption, empty symbols = desorption.

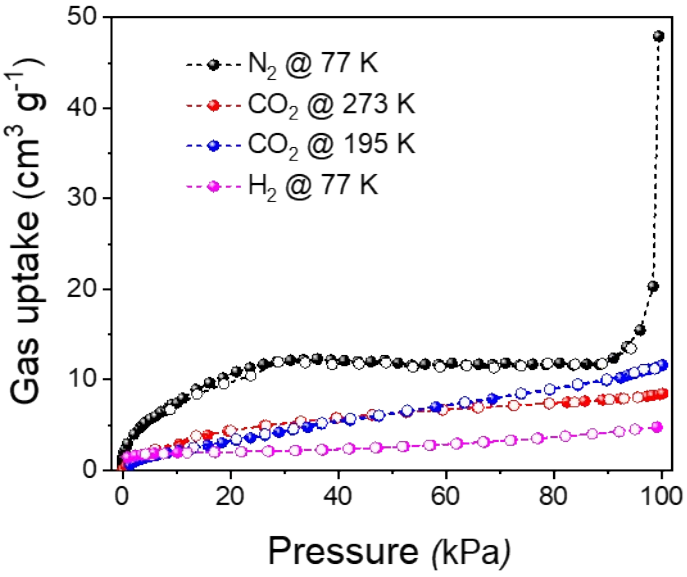

Fig. S40. Gas adsorption isotherms of the as-synthesized ZIF-8 foam. Filled symbols = adsorption, empty symbols = desorption.

Table S4. Summary of the porosity characteristics of ZIF-7 and ZIF-8 foams derived from ZIF-7 and ZIF-8 crystals. The porosity parameters of the melt-quenched ZIF glasses are provided for comparison.

Sample	BET model (N_2/77 K)			DFT model (CO_2/ 273 K)			CO_2 uptake (195 K) at 100 kPa ($cm^3\ g^{-1}$)	H_2 uptake (77 K) at 100 kPa ($cm^3\ g^{-1}$)	Ref.
	Surface area ($m^2\ g^{-1}$)	Total pore volume ($cm^3\ g^{-1}$)	N_2 uptake at 100 kPa ($cm^3\ g^{-1}$)	Surface area ($m^2\ g^{-1}$)	Total pore volume ($cm^3\ g^{-1}$)	CO_2 uptake at 100 kPa ($cm^3\ g^{-1}$)			
ZIF-7 crystal	-	-	-	7	0.002	1	3.40	1.60	This work
ZIF-7 foam	19	0.012	7.50	60	0.015	8.05	20.73	2.67	This work
ZIF-8 crystal	1438	0.826	534.39	133	0.031	16.85	86.05	151	This work
ZIF-8 foam	41	0.074	47.94	62	0.016	8.47	11.62	4.77	This work
ZIF-4 glass	-	-	-	-	-	-	-	-	20
ZIF-62 glass	-	-	-	-	-	20.1	-	9.3	19
ZIF-62 glass foam	2.83	0.005	3	-	-	30	-	-	16
ZIF-76 glass	-	-	-	375	0.12	35	-	-	12
ZIF-8/IL glass	16-17	0.001-0.003	5-10	-	-	10-15	-	-	2
ZIF-UC glass	-	-	-	-	-	18-42	-	-	21
MUV-24 glass	-	-	-	-	-	-	-	-	22

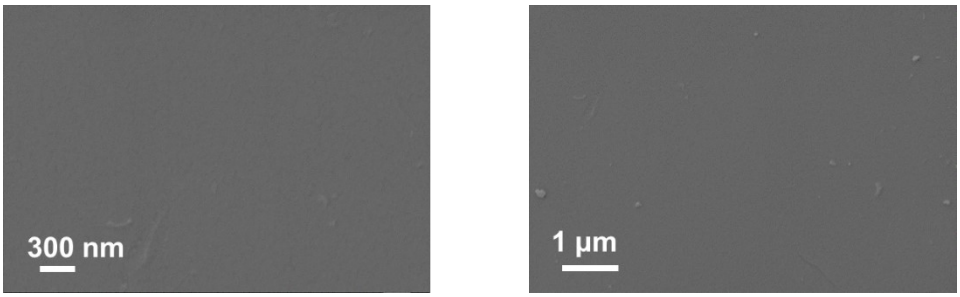

Fig. S41. SEM images of the as-fabricated membrane based on ZIF-7 foam observed at different areas.

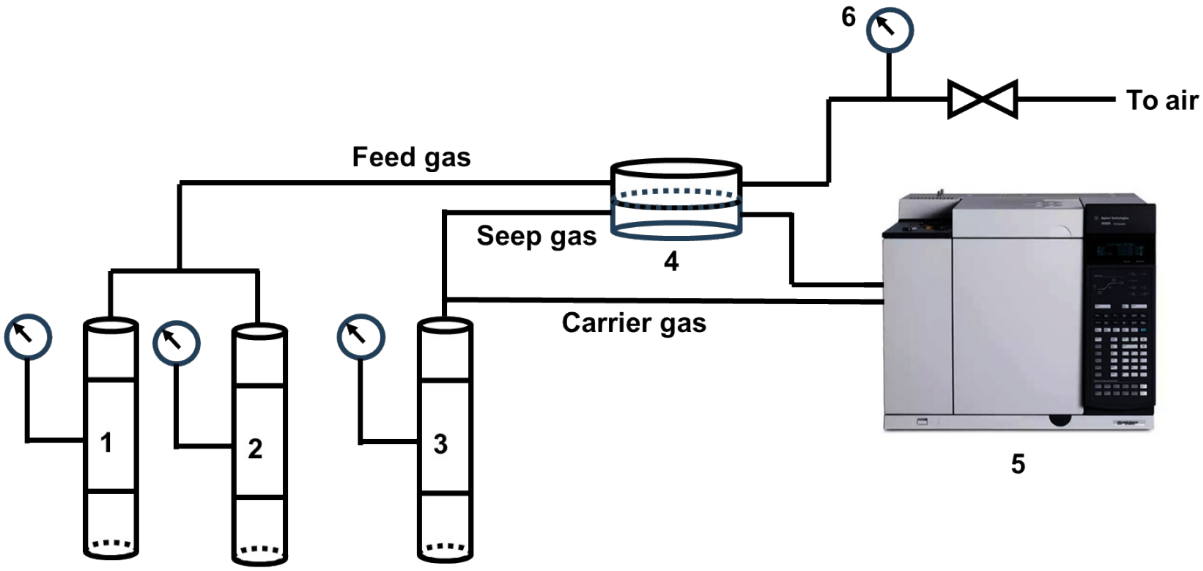

Fig. S42. Schematic diagram of the custom-made constant volume-variable pressure gas permeability test.

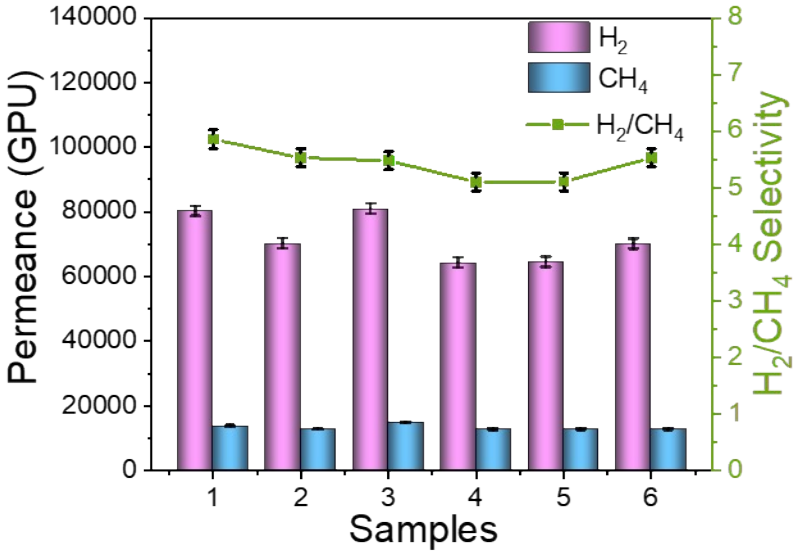

Fig. S43. Pure H_2 and CH_4 gas permeance and H_2/CH_4 selectivity of the as-fabricated membrane based on ZIF-8 foam that measured for six membranes with a thickness of 460 μm. The *x*-axis represents the sample number which was prepared under the same conditions.

Supplementary References

[1] Y. Peng, Y. Li, Y. Ban, H. Jin, W. Jiao, X. Liu and W. Yang, Metal-organic framework nanosheets as building blocks for molecular sieving membranes. *Science* 2014, **346,** 1356–1359.

[2] V. Nozari, C. Calahoo, J. M. Tuffnell, D. A. Keen, T. D. Bennett and L. Wondraczek, Ionic liquid facilitated melting of the metal-organic framework ZIF-8, *Nat. Commun.* 2021, **12,** 5703.

[3] P. Zhao, G. I. Lampronti, G. O. Lloyd, M. T. Wharmby, S. Facq, A. K. Cheetham and S. A. T. Redfern, Phase transitions in zeolitic imidazolate framework 7: the importance of framework flexibility and guest-induced instability, *Chem. Mater.* 2014, **26,** 1767–1769.

[4] M. A. Ali, M. A. Mohamed, X. Liu and J. Qiu, Reversible structural transformation of supramolecular inorganic-organic hybrid glass and zeolitic-imidazolate framework, *Mater. Chem. Front.* 2023, **7,** 6236–6246.

[5] M. A. Ali, X. Liu, H. T. Sun, J. Ren and J. Qiu, Metal inorganic–organic complex glass and fiber for photonic applications, *Chem. Mater.* 2022, **34,** 2476–2483.

[6] M. A. Ali, X. Liu, B. Xu, Y. Li, M. A. Mohamed, Y. Yue and J. Qiu, Vitrification and luminescence properties of metal–organic complexes, *ACS Mater. Lett.* 2022, **4,** 2613–2621.

[7] H. Wang, Z. Xiao, J. Yang, D. Lu, A. Kishen, Y. Li, Z. Chen, K. Que, Q. Zhang, X. Deng, X. Yang, Q. Cai, N. Chen, C. Cong, B. Guan, T. Li and X. Zhang, Oriented and ordered biomimetic remineralization of the surface of demineralized dental enamel using HAP@ACP nanoparticles guided by glycine, *Sci. Rep.* 2017, **7,** 40701.

[8] Y. S. Wei, Z. Fan, C. Luo and S. Horike, Desolvation of metal complexes to construct metal–organic framework glasses, *Nat. Synth*. 2024, **3,** 214–223.

[9] S. Sneddon, J. Kahr, A. F. Orsi, D. J. Price, D. M. Dawson, P. A. Wright and S. E. Ashbrook, Investigation of zeolitic imidazolate frameworks using ^{13}C and ^{15}N solid-state NMR spectroscopy, *Solid State Nucl. Magn. Reson.* 2017, **87,** 54–64.

[10] E. F. Baxter, T. D. Bennett, C. M. Draznieks, C. Gervais, F. Blanc and A. K. Cheetham, Combined experimental and computational NMR study of crystalline and amorphous zeolitic imidazolate frameworks, *Phys. Chem. Chem. Phys.* 2015, **17,** 25191–25196.

[11] C. I. Nieto, P. Cabildo, M. A. Garcı´a, R. M. Claramunt, I. Alkorta and J. Elguero, An experimental and theoretical NMR study of NH-benzimidazoles in solution and in the solid state: proton transfer and tautomerism, *Beilstein J. Org. Chem.* 2014, **10,** 1620–1629.

[12] C. Zhou, L. Longley, A. Krajnc, G. J. Smales, A. Qiao, I. Erucar, C. M. Doherty, A. W. Thornton, A. J. Hill, C. W. Ashling, O. T. Qazvini, S. J. Lee, P. A. Chater, N. J. Terrill, A. J. Smith, Y. Yue, G. Mali, D. A. Keen, S. G. Telfer and T. D. Bennett, Metal-organic framework glasses with permanent accessible porosity, *Nat. Commun.* 2018, **9,** 5042.

[13] A. Qiao, T. D. Bennett, H. Tao, A. Krajnc, G. Mali, C. M. Doherty, A. W. Thornton, J. C. Mauro, G. N. Greaves and Y. Yue, A metal-organic framework with ultrahigh glass-forming ability, *Sci. Adv.* 2018, **4,** eaao6827.

[14] R. S. K. Madsen, A. Qiao, J. Sen, I. Hung, K. Chen, Z. Gan, S. Sen and Y. Yue, Ultrahigh-field ^{67}Zn NMR reveals short-range disorder in zeolitic imidazolate framework glasses, *Science* 2020, **367,** 1473−1476.

[15] L. F. Beyme, M. Kloß, R. Pallach, S. Salamon, H. Moldenhauer, J. Landers, H. Wende, J. Debus and S. Henke, Porous purple glass –a cobalt imidazolate glass with accessible porosity from a meltable cobalt imidazolate framework, *J. Mater. Chem. A* 2019, **7**, 985–990.

[16] Z. Yang, Y. Belmabkhout, L. N. McHugh, D. Ao, Y. Sun, S. Li, Z. Qiao, T. D. Bennett, M. D. Guiver and C. Zhong, ZIF-62 glass foam self-supported membranes to address CH_4/N_2 separations, *Nat. Mater.* 2023, **22,** 888–894.

[17] Z. Fan, Y. S. Wei, H. Tabe, T. Nakatani, C. Das, H. Yamada and S. Horike, Formation of porosity toward acetylene upon vitrification of non-porous photochromic coordination polymer crystals, *Chem. Mater.* 2023, **35,** 3859–3866.

[18] R. Banerjee, A. Phan, B. Wang, C. Knobler, H. Furukawa, M. O'Keeffe and O. M. Yaghi, High-throughput synthesis of zeolitic imidazolate frameworks and application to CO_2 capture, *Science* 2008, **319,** 939–943.

[19] R. N. Widmer, G. I. Lampronti, S. Anzellini, R. Gaillac, S. Farsang, C. Zhou, A. M. Belenguer, C. W. Wilson, H. Palmer, A. K. Kleppe, M. T. Wharmby, X. Yu, S. M. Cohen, S. G. Telfer, S. A. T. Redfern, F. X. Coudert, S. G. MacLeod and T. D. Bennett, Pressure promoted low-temperature melting of metal–organic frameworks, *Nat. Mater.* 2019, **18,** 370–376.

[20] T. D. Bennett, Y. Yue, P. Li, A. Qiao, H. Tao, N. G. Greaves, T. Richards, G. I. Lampronti, S. A. T. Redfern, F. Blanc, O. K. Farha, J. T. Hupp, A. K. Cheetham and D. A. Keen, Melt-quenched glasses of metal−organic frameworks, *J. Am. Chem. Soc.* 2016, **138,** 3484−3492.

[21] J. Hou, M. L. R. Gómez, A. Krajnc, A. McCaul, S. Li, A. M. Bumstead, A. F. Sapnik, Z. Deng, R. Lin, P. A. Chater, D. S. Keeble, D. A. Keen, D. Appadoo, B. Chan, V. Chen, G. Mali and T. D. Bennett, Halogenated metal–organic framework glasses and liquids, *J. Am. Chem. Soc.* 2020, **142,** 3880–3890.

[22] L. L. Alcaide, R. S. Christensen, D. A. Keen, J. L. Jordá, I. B. Alcázar, A. F. Aliaga and G. M. Espallargas, Meltable, glass-forming, iron zeolitic imidazolate frameworks, *J. Am. Chem. Soc.* 2023, **145,** 11258–11264.

[23] A. W. Thornton, K. E. Jelfs, K. Konstas, C. M. Doherty, A. J. Hill, A. K. Cheethamc and T. D. Bennett, Porosity in metal–organic framework glasses, *Chem. Commun.* 2016, **52,** 3750–3753.